RESEARCH ARTICLE SUMMARY

NEURODEGENERATION

Restoring hippocampal glucose metabolism rescues cognition across Alzheimer's disease pathologies

Paras S. Minhas†, Jeffrey R. Jones†, Amira Latif-Hernandez†, Yuki Sugiura, Aarooran S. Durairaj, Qian Wang, Siddhita D. Mhatre, Takeshi Uenaka, Joshua Crapser, Travis Conley, Hannah Ennerfelt, Yoo Jin Jung, Ling Liu, Praveena Prasad, Brenita C. Jenkins, Yeonglong Albert Ay, Matthew Matrongolo, Ryan Goodman, Traci Newmeyer, Kelly Heard, Austin Kang, Edward N. Wilson, Tao Yang, Erik M. Ullian, Geidy E. Serrano, Thomas G. Beach, Marius Wernig, Joshua D. Rabinowitz, Makoto Suematsu, Frank M. Longo, Melanie R. McReynolds, Fred H. Gage, Katrin I. Andreasson*

INTRODUCTION: Alzheimer's disease (AD) is an age-associated neurodegenerative disorder characterized by a progressive and irreversible loss of synapses and neural circuitry. Major pathophysiologic processes that contribute to synaptic loss, including disrupted proteostasis, accumulation of misfolded amyloid and tau, and microglial dysfunction, are being vigorously investigated with the goal of identifying disease-modifying therapies. However, coincident with these distinct pathologies is a sustained decline in cerebral glucose metabolism, with recent proteomics revealing a marked disruption of astrocytic and microglial metabolism in AD subjects.

RATIONALE: Astrocytes generate lactate that is exported to neurons to fuel mitochondrial respiration and support synaptic activity. Recent studies have suggested a role for indoleamine-2,3-dioxygenase 1 (IDO1), an enzyme expressed in astrocytes, in multiple neurodegenerative disorders, including AD. IDO1 is the rate-limiting enzyme in the conversion of tryptophan (TRP) to kynurenine (KYN), a metabolite that elicits immune suppression in inflammatory and neoplastic contexts through interaction with the aryl-hydrocarbon receptor (AhR). IDO1 activity is significantly up-regulated by a variety of immunogenic stimuli, and, in the brain, IDO1 is expressed in astrocytes and microglia but not in neurons, where levels can increase in response to inflammatory stimuli.

RESULTS: We report that inhibition of IDO1 and production of KYN rescues hippocampal synaptic plasticity and memory function in preclinical models of amyloid and tau pathology by restoring astrocytic metabolic support of neurons. Activation of IDO1 in astrocytes by amyloid β and tau oligomers, two major pathologic effectors in AD, increases KYN and suppresses glycolysis in an AhR-dependent manner. Conversely, pharmacological IDO1 inhibition restores astrocytic glycolysis and lactate production. In amyloid-producing APP^{Swe}-$PS1^{\Delta E9}$ and 5XFAD mice and in tau-producing P301S mice, IDO1 inhibition improves hippocampal glucose metabolism, as shown by metabolomic and MALDI-MS (matrix-assisted laser desorption ionization–mass spectrometry) analyses, and restores spatial memory. IDO1 blockade also rescues hippocampal long-term potentiation in a monocarboxylate transporter–dependent manner, suggesting that IDO1 activity disrupts astrocytic metabolic support of neurons. Indeed, in vitro mass labeling of human astrocytes demonstrated that IDO1 regulates astrocyte generation of lactate that is then taken up by human neurons. In cocultures of astrocytes and neurons derived from AD subjects, deficient astrocyte lactate production and transfer to neurons was corrected by IDO1 inhibition, resulting in improved neuronal glucose metabolism.

CONCLUSION: In addition to uncovering a previously uncharacterized role of IDO1 in brain glucose metabolism, our study highlights the potential of brain penetrant IDO1 inhibitors, developed as an adjunctive therapy for cancer, to be repurposed for treating neurodegenerative diseases such as AD. This study also reveals a general mechanism contributing to neuronal dysfunction that cuts across distinct pathologies. In addition to AD, manipulation of IDO1 may be relevant to Parkinson's disease dementia, which is characterized by amyloid accumulation in addition to α-synuclein, as well as the broad spectrum of tauopathies. There is the possibility that deficient astrocytic glucose metabolism could also underlie other neurodegenerative diseases characterized by the accumulation of other misfolded proteins where increases in kynurenine pathway metabolites have been observed. ■

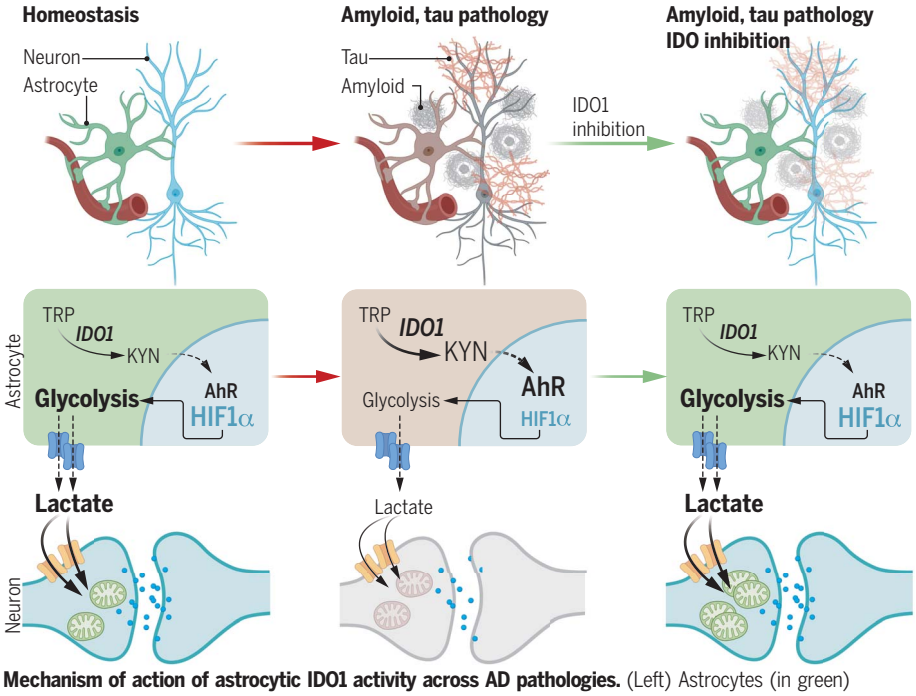

Mechanism of action of astrocytic IDO1 activity across AD pathologies. (Left) Astrocytes (in green) generate lactate, and glycolytic gene expression is partly regulated by hypoxia-inducible factor 1-α (HIF1α). Sufficient lactate is transferred from the astrocyte to the neuron (in blue) to fuel neuronal mitochondrial respiration and synaptic activity. (Middle) Astrocytic IDO1 generation of KYN increases, disrupting the balance between AhR and HIF1α nuclear signaling and reducing astrocytic glycolysis, lactate production, and metabolic support of neuronal activity. (Right) Decreased astrocyte KYN restores glycolysis and metabolic support of neurons and reduces the severity of amyloid and tau pathologies. [Figure created with BioRender.com]

The list of author affiliations is available in the full article online.
*Corresponding author. Email: kandreas@stanford.edu
†These authors contributed equally to this work.
Cite this article as P. S. Minhas *et al.*, *Science* **385**, eabm6131 (2024). DOI: 10.1126/science.abm6131

READ THE FULL ARTICLE AT
https://doi.org/10.1126/science.abm6131

RESEARCH ARTICLE

NEURODEGENERATION

Restoring hippocampal glucose metabolism rescues cognition across Alzheimer's disease pathologies

Paras S. Minhas[1,2]†, Jeffrey R. Jones[3]†, Amira Latif-Hernandez[1]†, Yuki Sugiura[4,5,6], Aarooran S. Durairaj[1], Qian Wang[1], Siddhita D. Mhatre[1], Takeshi Uenaka[7], Joshua Crapser[1], Travis Conley[1], Hannah Ennerfelt[1], Yoo Jin Jung[1], Ling Liu[8,9], Praveena Prasad[10], Brenita C. Jenkins[10], Yeonglong Albert Ay[1], Matthew Matrongolo[1], Ryan Goodman[3], Traci Newmeyer[3], Kelly Heard[3], Austin Kang[3], Edward N. Wilson[1], Tao Yang[1], Erik M. Ullian[11], Geidy E. Serrano[12], Thomas G. Beach[12], Marius Wernig[7,13], Joshua D. Rabinowitz[8,9], Makoto Suematsu[4,5], Frank M. Longo[1,2], Melanie R. McReynolds[8,9,10], Fred H. Gage[3], Katrin I. Andreasson[1,2,14,15]*

Impaired cerebral glucose metabolism is a pathologic feature of Alzheimer's disease (AD), with recent proteomic studies highlighting disrupted glial metabolism in AD. We report that inhibition of indoleamine-2,3-dioxygenase 1 (IDO1), which metabolizes tryptophan to kynurenine (KYN), rescues hippocampal memory function in mouse preclinical models of AD by restoring astrocyte metabolism. Activation of astrocytic IDO1 by amyloid β and tau oligomers increases KYN and suppresses glycolysis in an aryl hydrocarbon receptor–dependent manner. In amyloid and tau models, IDO1 inhibition improves hippocampal glucose metabolism and rescues hippocampal long-term potentiation in a monocarboxylate transporter–dependent manner. In astrocytic and neuronal cocultures from AD subjects, IDO1 inhibition improved astrocytic production of lactate and uptake by neurons. Thus, IDO1 inhibitors presently developed for cancer might be repurposed for treatment of AD.

Alzheimer's disease (AD) is an age-associated neurodegenerative disorder characterized by the progressive and irreversible loss of synapses and neural circuitry (*1*). Major pathophysiologic processes that contribute to synaptic loss, including disrupted proteostasis, accumulation of misfolded amyloid and tau, and microglial dysfunction, are being investigated with the goal of identifying disease-modifying therapies. However, coincident with these distinct pathologies is a sustained decline in cerebral glucose metabolism (*2*, *3*), with recent proteomics revealing a marked disruption of astrocytic and microglial metabolism in individuals with AD (*4*). Astrocytes, which exist in approximately a 1:1 ratio to neurons (*5*), are essential for regulation of neurotransmitter concentrations and bioenergetic support of neurons. Specifically, astrocytes can generate lactate that is exported to neurons to fuel mitochondrial respiration and support synaptic activity (*6*–*8*).

Recent studies have suggested a role for indoleamine-2,3-dioxygenase 1 (IDO1), an enzyme expressed in astrocytes that metabolizes tryptophan (TRP) to kynurenine (KYN), in multiple neurodegenerative disorders, including AD (*9*). IDO1 is the rate-limiting enzyme in the conversion of TRP to KYN, a metabolite that elicits immune suppression in inflammatory and neoplastic contexts through interaction with the aryl hydrocarbon receptor (AhR) (*10*). IDO1 activity is up-regulated in the context of multiple immunogenic stimuli, including lipopolysaccharide and proinflammatory factors; in the brain, IDO1 is expressed in astrocytes and microglia but not in neurons, and concentrations increase in response to inflammatory stimuli (*11*, *12*). Here, we report that KYN generated by IDO1 suppresses astrocytic lactate transfer to neurons in mouse models of AD pathology and human induced pluripotent stem cell (iPSC)–derived astrocytes from patients with late-onset AD. Genetic deletion of IDO1 or pharmacologic inhibition with a brain-penetrant IDO1 inhibitor restored hippocampal glucose metabolism and spatial memory in preclinical models of amyloid β (Aβ) and tau accumulation, suggesting that these distinct pathologies share a common metabolic deficit.

[1]Department of Neurology and Neurological Sciences, Stanford University School of Medicine, Stanford, CA, 94305, USA. [2]Wu Tsai Neurosciences Institute, Stanford University, Stanford, CA 94305, USA. [3]Laboratory of Genetics, The Salk Institute for Biological Studies, La Jolla, CA 92037, USA. [4]Central Institute for Experimental Medicine and Life Science, Keio University, 3-25-12 Tonomachi, Kawasaki-ku, Kawasaki 210-0821, Japan. [5]WPI-Bio2Q Research Center, Keio University, 3-25-12 Tonomachi, Kawasaki-ku, Kawasaki 210-0821 Japan. [6]Center for Cancer Immunotherapy and Immunobiology, Kyoto University Graduate School of Medicine, Kyoto 606-8501, Japan. [7]Department of Pathology, Stanford University School of Medicine, Stanford, CA 94305, USA. [8]Lewis Institute for Cancer Research, Princeton University, Princeton, NJ 08544, USA. [9]Department of Chemistry, Princeton University, Princeton 08544 NJ, USA. [10]Department of Biochemistry and Molecular Biology, Huck Institutes of the Life Sciences, Pennsylvania State University, University Park, PA 16802, USA. [11]Department of Ophthalmology, University of California, San Francisco, San Francisco, CA 94143, USA. [12]Civin Laboratory for Neuropathology, Banner Sun Health Research Institute, Sun City, AZ 85351, USA. [13]Department of Chemical and Systems Biology, Stanford University, Stanford, CA 94305, USA. [14]Chan Zuckerberg Biohub, San Francisco, CA 94158, USA. [15]The Phil and Penny Knight Initiative for Brain Resilience at the Wu Tsai Neurosciences Institute, Stanford University, CA 94305, USA.
*Corresponding author. Email: kandreas@stanford.edu
†These authors contributed equally to this work.

IDO1 inhibition restores astrocytic bioenergetic responses to amyloid peptide and tau oligomers

We investigated whether IDO1 activity functioned in astrocytic responses to 42-residue Aβ ($Aβ_{42}$) oligomers (oAβ) and tau oligomers (oTau), the two major neurotoxic pathologies in AD. Mouse primary astrocytes showed a substantial induction of IDO1 mRNA expression and prominent IDO1-dependent KYN production in response to oAβ, oTau, and the combination of oAβ and oTau (oAβ+oTau) (Fig. 1, A to D, and fig. S1, A to C). We also observed AD pathology–induced activation of IDO1 and KYN production in human iPSC-derived astrocytes (iAstrocytes) (*13*) (Fig. 1E and fig. S1D), suggesting a conserved IDO1 response to Aβ and tau oligomers across mouse and human astrocytes. IDO1-mediated KYN generation was suppressed by pretreatment with the selective IDO1 inhibitor PF06840003 (PF068) (*14*). We administered PF068 in combination with ^{13}C-labeled TRP and traced KYN in mouse and human astrocytes; we found elevated concentrations of TRP-derived KYN in response to oAβ+oTau in both mouse and human astrocytes, confirming that oAβ+oTau increased KYN specifically through activation of IDO1 (Fig. 1D and fig. S1, E to G).

We then investigated the downstream effects of IDO1 activation in astrocytes. KYN binds to the AhR and triggers translocation of the AhR to the nucleus (*10*, *15*). In the nucleus, the AhR dimerizes with the AhR nuclear translocator (ARNT) to regulate transcriptional responses (fig. S2A). We tested whether stimulation of astrocytes with oAβ+oTau induced IDO1-dependent AhR:ARNT binding. Coimmunoprecipitation of AhR and ARNT increased in response to oAβ+oTau, and this increase was inhibited by PF068 (Fig. 1F), suggesting that oAβ+oTau activates IDO1 and induces AhR:ARNT binding. Orthogonal validation using immunohistochemical detection of AhR confirmed that IDO1 promotes AhR translocation to astrocyte nuclei (Fig. 1G and fig. S2B).

In the nucleus, ARNT concentrations are limiting because ARNT can also bind to hypoxia-inducible factor 1-α (HIF1α; fig. S2A) (*16*), a transcription factor that regulates glycolytic gene transcription and increases generation of lactate (*17*). To assess astrocytic AhR-ARNT versus HIF1α-ARNT gene expression, we examined AhR versus HIF1α transcriptional responses to oAβ+oTau stimulation in mouse astrocytes with or without incubation with PF068. As expected, astrocytic AhR gene transcription increased after oAβ+oTau stimulation but was reduced with IDO1 inhibition (Fig. 1H). Conversely, IDO1 inhibition increased HIF1α-regulated

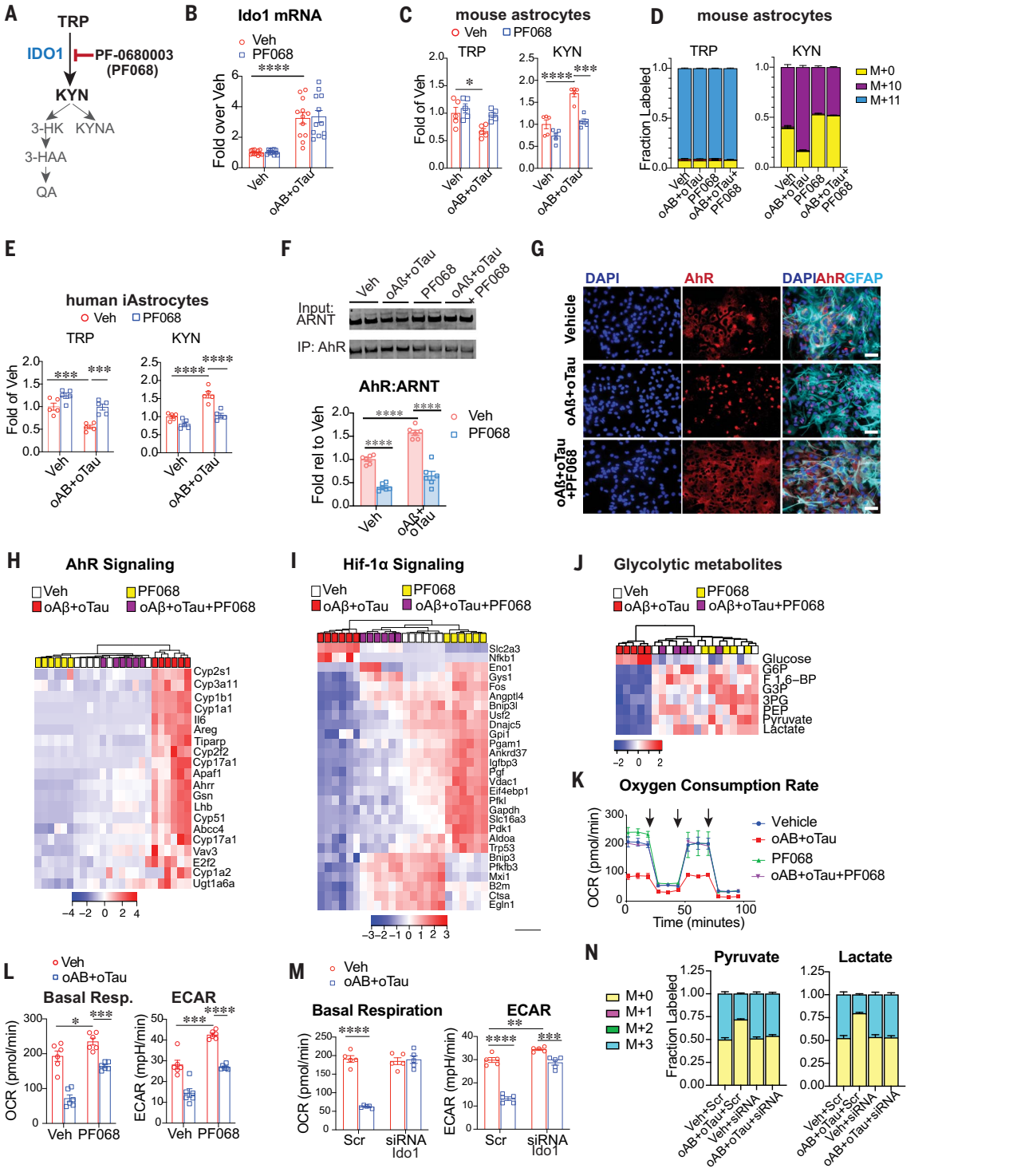

Fig. 1. Activation of astrocytic IDO1 in response to Aβ_{42} and tau oligomers suppresses astrocytic glycolysis. Data are mean ± SEM and were analyzed using two-way analysis of variance (ANOVA) with Tukey post hoc tests; *P < 0.05, **P < 0.01, ***P < 0.001, and ****P < 0.0001. Hierarchical clustering is represented in terms of distance from the mean, or z-score. (**A**) The kynurenine pathway: The essential amino acid TRP is metabolized to KYN by IDO1. The specific IDO1 inhibitor PF06840003 (PF068) prevents KYN production. 3-HK, 3-hydroxykynurenine; 3-HAA, 3-hydroxyanthranilic acid. (**B**) Quantitative reverse transcription PCR (qRT-PCR) of *Ido1* expression in mouse astrocytes stimulated with vehicle or oAβ+oTau (100 nM, 20 hours) with or without PF068 (100 nM, 20 hours; n = 12 per group). (**C**) Primary mouse astrocytes were stimulated with vehicle (Veh) or oAβ+oTau (100 nM, 20 hours) with or without PF068 (100 nM, 20 hours). LC-MS quantification of TRP and KYN (n = 5 per group). (**D**) Isotope tracing of ^{13}C-TRP [M+11] to KYN [M+10] in mouse astrocytes (n = 5 per group). Similar mass labeling occurs in human astrocytes (fig. S1G). (**E**) iPSC-derived human iAstrocytes were stimulated with vehicle or oAβ+oTau (100 nM, 20 hours) with or without PF068 (100 nM, 20 hours). LC-MS quantification of TRP and KYN (n = 5 per group). (**F**) Coimmunoprecipitation (CoIP) of AhR and ARNT in mouse astrocytes. A representative immunoblot is shown at the top. Quantification of coimmunoprecipitated AhR:ARNT in

astrocytes treated with oAβ+oTau with or without PF068 (100 nM, 20 hours) is shown at the bottom. (**G**) Immunocytochemical detection of AhR (red) in primary mouse astrocytes (GFAP, blue) shows nuclear localization after stimulation with oAβ+oTau (100 nM, 20 hours) that is prevented with PF068 (100 nM, 20 hours). Scale bars are 50 μM. DAPI, 4′,6-diamidino-2-phenylindole. (**H**) qRT-PCR of AhR-dependent gene transcripts that are significantly altered in mouse astrocytes with or without oAβ+oTau ($q < 0.05$). (**I**) qRT-PCR of Hif-1α-dependent gene transcripts significantly altered in mouse astrocytes with or without oAβ+oTau ($q < 0.05$). (**J**) LC-MS of glycolytic metabolites in primary astrocytes with or without oAβ+oTau (100 nM, 20 hours) and with or without PF068 (100 nM, 20 hours); $n = 5$ per group). (**K**) Realtime oxygen consumption rate (OCR) in mouse astrocytes with or without oAβ+oTau (100 nM, 20 hours) and with or without PF068 (100 nM, 20 hours; $n = 6$ per group). Cells were treated sequentially with 1 μM oligomycin, 2 μM carbonyl cyanide-p-trifluoromethoxyphenylhydrazone (FCCP), and 0.5 μM rotenone and antimycin, as indicated by the three arrows. (**L**) Quantification of basal respiration (left) and extracellular acidification rate (ECAR) (right) from (K); $n = 6$ per group. (**M**) Mouse astrocytes were transfected with either scrambled siRNA (Scr) or siRNA to Ido1. Shown are quantifications of basal respiration (left) and ECAR (right); $n = 5$ per group. (**N**) Fraction labeled of pyruvate and lactate from isotope-tracing of ^{13}C-glucose administered to mouse astrocytes transfected with either scrambled siRNA (Scr) or siRNA to Ido1 and stimulated with vehicle or oAβ+oTau (100 nM, 20 hours; $n = 5$ per group).

glycolytic gene expression in resting astrocytes and reversed suppression of HIF1α-regulated transcripts in oAβ+oTau–stimulated astrocytes (Fig. 1I and fig. S2, C and D). Indeed, IDO1 inhibition restored glycolytic intermediates and lactate, glycolysis [measured as extracellular acidification rate (ECAR)], and mitochondrial oxidative phosphorylation (measured as basal respiration) in oAβ+oTau–stimulated astrocytes (Fig. 1, J to L, and fig. S2E). The metabolic effect of IDO1 inhibition on astrocyte bioenergetics was validated using small interfering RNA (siRNA) to knock down expression of IDO1 (fig. S3, A and B). IDO1 knockdown phenocopied pharmacologic inhibition of IDO1 and restored basal respiration, ECAR, and glycolytic intermediates, including lactate, in astrocytes stimulated with oAβ+oTau (Fig. 1, M and N, and fig. S3, C to E). Conversely, application of exogenousKYN to mouse astrocytes elicited a dose-dependent decrease in basal respiration and ECAR and suppressed generation of glycolytic and tricarboxylic acid (TCA) intermediates in astrocytes stimulated with oAβ+oTau (Fig. 2, A to C, and fig. S3F). Taken together, these data indicate that astrocytic glucose metabolism is disrupted by oAβ+oTau through an IDO1-dependent mechanism.

To further confirm the role of IDO1 and AhR in suppressing astrocytic glycolytic responses to oAβ+oTau, we transfected astrocytes with a short hairpin RNA (shRNA) to AhR. Quantitative immunoblotting confirmed knockdown of AhR protein concentrations (fig. S3G) and Seahorse bioenergetic analysis revealed that AhR knockdown prevented oAβ+oTau–driven deficits in astrocytic glucose metabolism (Fig. 2, D and E). To verify that AhR knockdown rescued glucose metabolism, we performed ^{13}C-glucose isotope tracing and observed a rescue of glucose incorporation into downstream glycolytic intermediates in AhR-deficient astrocytes stimulated with oAβ+oTau (Fig. 2F and fig. S3H). Immune factor profiling of activated astrocytes showed no effect of IDO1 inhibition (fig. S3I). Thus, KYN-dependent AhR signaling suppresses glucose metabolism in astrocytes exposed to oAβ+oTau. These data suggest that increased IDO1 activity may negatively affect astrocytic metabolic support of neurons in AD.

IDO1 inhibition rescues long-term memory in amyloid models of AD pathology

Astrocytes are the major repository of glycogen in the brain, and glycogen can be rapidly catabolized to lactate and exported to fuel neuronal mitochondrial respiration and synaptic activity (*6*–*8*). Learning and memory are enabled by astrocyte-derived lactate (*8*, *18*–*21*). Given the role of astrocytic lactate in supporting neuronal metabolism, we hypothesized that IDO1 inhibition in astrocytes might improve hippocampal memory deficits and synaptic plasticity in models of AD pathology.

We first confirmed the absence of IDO1 activity in primary mouse neurons as compared with astrocytes. IDO1 inhibition with PF068 elicited a dose-response increase in glycolysis and mitochondrial respiration in astrocytes but not neurons (Fig. 2, G and H, and fig. S4, A and B). We then assessed in vivo effects of the brain penetrant IDO1 inhibitor PF068 on hippocampal KYN and lactate concentrations in 6-month-old wild-type (WT) mice 4 hours after PF068 administration [0 to 15 mg per kg body weight (mg/kg) dose-response given orally]. IDO1 inhibition reduced hippocampal KYN and reciprocally increased lactate in a dose-dependent manner (Fig. 2I). We then tested the effects of PF068 in two mutant amyloid precursor protein (APP) mouse models that accumulate misfolded $A\beta_{42}$ peptides: the *APP*^{Swe}-*PS1*$^{\Delta E9}$ (APP/PS1) (*22*) and the 5XFAD (*23*) models. Hippocampal KYN increased in both mutant APP models, and this increase was blocked by PF068 (15 mg/kg given orally for 1 month), indicating that IDO1 activation is associated with $A\beta_{42}$ accumulation in vivo (Fig. 2, J and L, and fig. S4, C and D). Hippocampal lactate was reduced in both models in an IDO1-dependent manner (Fig. 2, K and M), suggesting a role for IDO1 and KYN generation in regulating hippocampal glucose metabolism in mouse models of amyloid accumulation.

We then tested whether IDO1 activity contributed to the well-established spatial memory and synaptic deficits observed in mutant APP models. IDO1 inhibition with PF068 reversed deficits in hippocampal-dependent spatial memory in the Barnes maze and novel object recognition (NOR) tasks in APP/PS1 mice (Fig. 3, A to C, and fig. S5, A to C). We also assessed hippocampal synaptic plasticity by measuring long term potentiation (LTP) at the CA3 to CA1 Schaffer collateral pathway in mouse brain slices. In line with the behavioral findings, IDO1 inhibition reversed deficits in LTP (*24*), a cellular indicator of learning and memory, in APP/PS1 mouse–derived brain slices (Fig. 3D and fig. S5D). Genetic ablation of IDO1 in APP/PS1 mice was produced by serial crossing of APP/PS1 mice with *Ido1*$^{-/-}$ mice; IDO1 deletion also rescued hippocampal spatial memory in the Morris water maze task (Fig. 3E). In line with pharmacologic inhibition in this model (Fig. 2K), genetic deletion of IDO1 also reduced KYN and conversely increased lactate in the hippocampus (Fig. 3, F and G, and fig. S5J). Spatial memory and hippocampal plasticity were also rescued in a second model of amyloid deposition, the 5XFAD model (Fig. 3, H to J, and fig. S5, E to I). For both models, IDO1 inhibition did not affect total amounts of cerebral $A\beta_{40}$ and $A\beta_{42}$, as measured by guanidine extraction of both soluble and insoluble Aβ peptides (fig. S5, K to M). However, Aβ peptide accumulation in the subiculum of thioflavin S (ThioS)–positive dense core plaques and 6E10-positive diffuse plaques decreased after pharmacologic inhibition in 5XFAD mice (Fig. 3, K and L), suggesting an effect on the aggregation state of amyloid. Accumulation of the synaptic protein BACE1, which cleaves APP, is considered a marker of dystrophic neurites (*25*); amounts of BACE1 were also reduced after IDO1 inhibition in 5XFAD mice, in line with the observed behavioral rescue. Astrocyte activation, as measured by glial fibrillary acidic protein (GFAP) integrated density, was not modulated by IDO1 inhibition (fig. S5N).

We then investigated transcriptional changes in the hippocampus of 5XFAD mice that resulted from inhibition of KYN-AhR signaling. Based on our previous data indicating that IDO1 is present in astrocytes and not in neurons (fig. S4, A and B), we indirectly assessed the effects of IDO1 inhibition on astrocytes in vivo and examined AhR and HIF1α transcriptional responses in the hippocampi of 5- to 6-month-old 5XFAD mice treated with PF068 (15 mg/kg for 4 weeks) (Fig. 3, M and N). IDO1 inhibition reduced AhR-regulated transcripts and

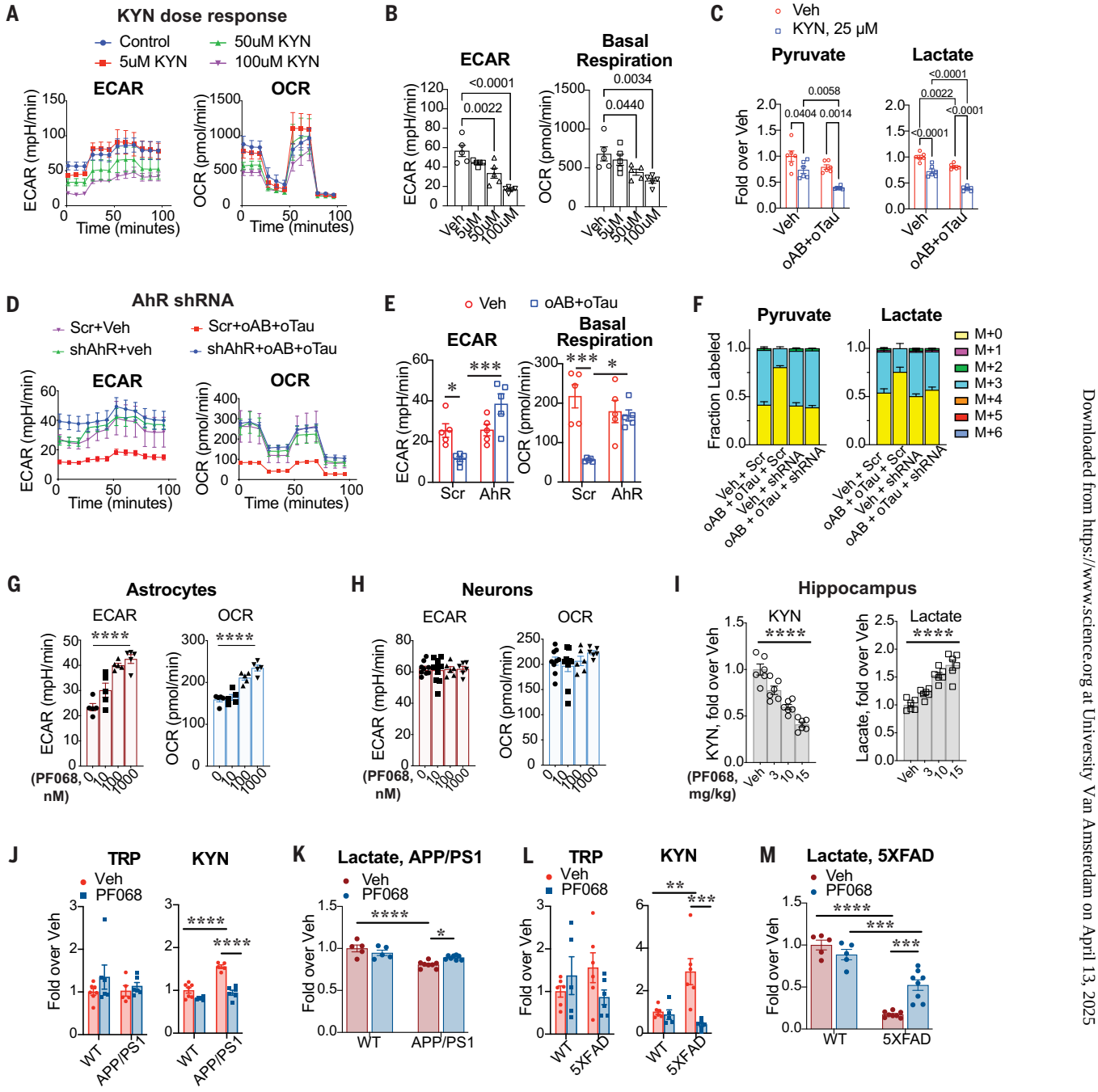

Fig. 2. IDO1 inhibition regulates lactate production in astrocytes and in the hippocampus of mutant APP mice. Data are mean ± SEM and were analyzed using two-way ANOVA with Tukey post hoc tests; *P < 0.05, **P < 0.01, ***P < 0.001, and ****P < 0.0001, unless otherwise specified. (**A**) Real-time ECAR and OCR tracings in mouse astrocytes stimulated with increasing concentrations of KYN (n = 5 per group, 20 hours). (**B**) Quantification of ECAR and basal respiration from (A), analyzed using one-way ANOVA with Tukey post hoc test (n = 5 per group). (**C**) LC-MS quantification of pyruvate and lactate in mouse astrocytes stimulated with or without oAβ+oTau (100 nM each, 20 hours) and either supplemented with KYN or not (25 mM, 20 hours). (**D**) Real-time OCR and ECAR traces in mouse astrocytes transfected with shRNA to AhR and stimulated with vehicle or oAβ+oTau (100 nM each, 20 hours; n = 5 per group). (**E**) Mouse astrocytes were transfected with either scrambled shRNA (Scr) or shRNA to AhR (AhR). Shown are quantifications of ECAR (left) and basal respiration (right); n = 5 per group. (**F**) Isotope-tracing of ^{13}C-glucose administration and quantification of pyruvate and lactate in mouse astrocytes transfected with either shRNA (Scr) or shRNA to AhR and stimulated with vehicle or oAβ+oTau (100 nM each, 20 hours; n = 5 per group). (**G**) Real-time changes in ECAR and OCR in mouse astrocytes stimulated with increasing doses of PF068 (20 hours; n = 5 group). Data were analyzed using one-way ANOVA with Tukey post hoc test; ****P < 0.001. (**H**) Real-time changes in ECAR and OCR in mouse hippocampal neurons stimulated with increasing doses of PF068 (n = 6 to 9 per group, 20 hours). (**I**) LC-MS quantification of hippocampal KYN and lactate in 6-month-old WT mice (n = 6 mice per group) treated with increasing doses of PF068 for 4 hours. Data were analyzed using one-way ANOVA with Tukey post hoc test; ****P < 0.001. (**J**) Fold change of hippocampal TRP and KYN in WT versus APP/PS1 mice treated with either vehicle or PF068 at a dosage of 15 mg/kg per day orally for 1 month (n = 5 to 7 per group). (**K**) Fold change of hippocampal lactate in APP/PS1 male mice from (J). (**L**) Fold change of hippocampal TRP and KYN in 5XFAD female mice with or without PF068 at a dosage of 15 mg/kg per day orally for 1 month (n = 5 or 6 per group). (**M**) Fold change of hippocampal lactate in 5XFAD female mice from (L).

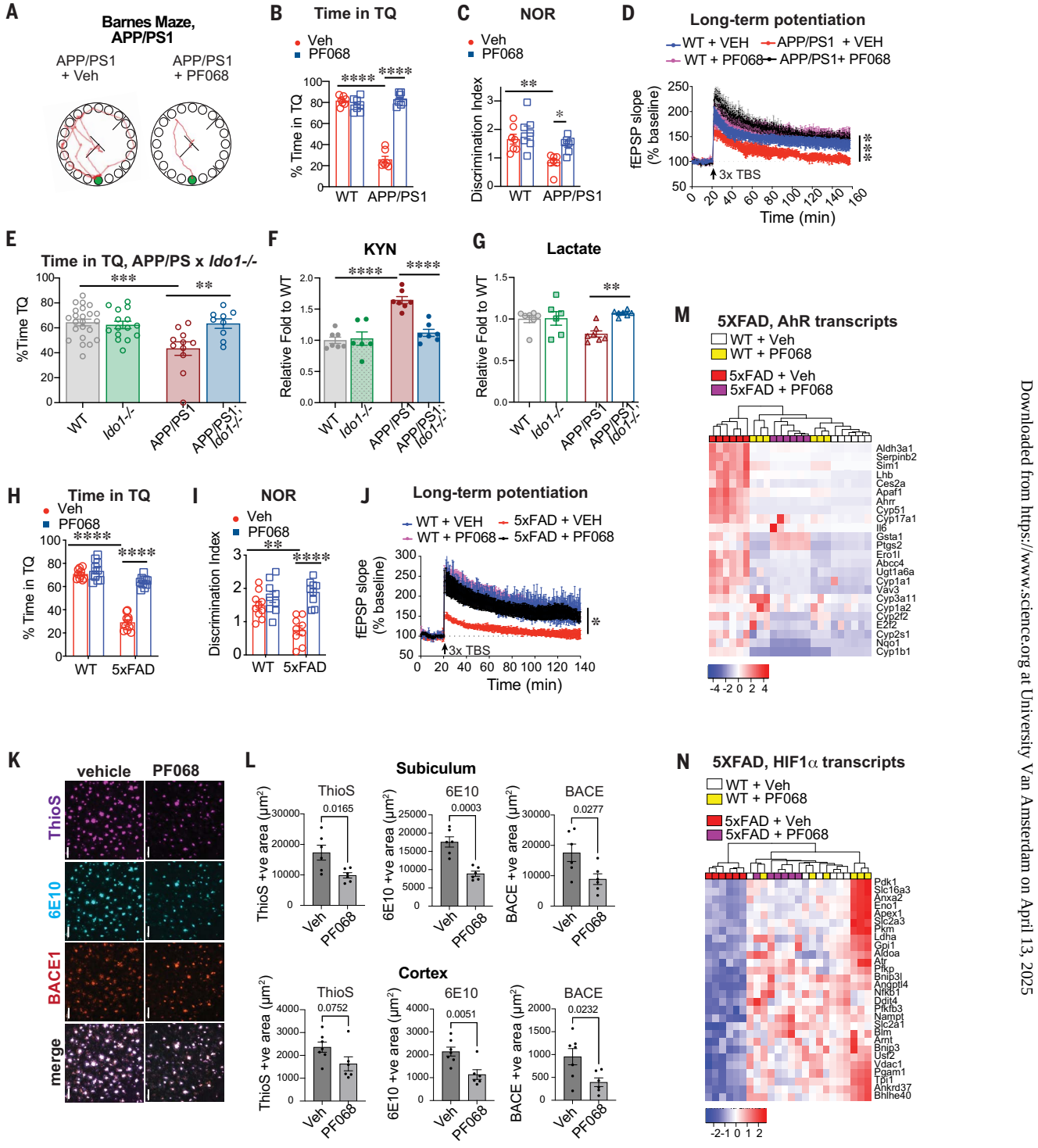

Fig. 3. IDO1 inhibition restores hippocampal memory and LTP in mutant APP models. WT and 5XFAD mice (5- to 6-month-old females per group) and WT and APP/PS1 mice (10- to 12-month-old males per group) were treated with vehicle or PF068 (15 mg/kg per day for 1 month); APP/PS1 mice were crossed onto an *Ido1* null background to generate APP/PS1 mice deficient in *Ido1*. Data are mean ± SEM and were analyzed using two-way ANOVA with Tukey post hoc tests; **P* < 0.05, ***P* < 0.01, ****P* < 0.001, and *****P* < 0.0001, unless otherwise specified. Hierarchical clustering is represented in terms of distance from the mean, or z-score. (**A**) Representative tracings of the test trial day in the Barnes maze in APP/PS1 male mice with or without PF068; escape hole in the target quadrant (TQ) is in green. (**B**) Percentage of time in the TQ from (A) (*n* = 9 or 10 mice per group). (**C**) Discrimination index in the NOR task for the number of interactions with the novel object in APP/PS1 male mice with or without PF068 (*n* = 9 or 10 mice per group). (**D**) LTP, measured as the change in field excitatory postsynaptic potential (fEPSP) in the CA1 hippocampal region over 150 min in APP/PS1 male mice with or without PF068 (15 mg/kg per day for 1 month). Three episodes of theta-burst stimulation (3× TBS; black arrows) were applied. Data were analyzed using two-way ANOVA, effects of time, and genotype, $P < 0.0001$; and Sidak's multiple comparisons test with Geisser-Greenhouse correction, ***$P < 0.05$ (*n* = 8 or 9 slices, 4 or 5 mice per group). (**E**) Morris water maze testing and time in the TQ for 10- to 12-month-old male APP/PS1 mice with *Ido1* deletion (*n* = 11 to 23 mice per group). (**F**) Fold

change of KYN in hippocampus relative to WT mice in APP/PS1 male mice with or without *Ido1* deletion (n = 6 or 7 mice per group). (**G**) Fold change of lactate in hippocampus of APP/PS1 male mice with or without *Ido1* deletion (n = 6 or 7 mice per group) relative to WT mice. (**H**) Quantification of time in the Barnes maze TQ for 5XFAD female mice with or without PF068 (n = 10 mice per group). (**I**) Discrimination index in the NOR task in 5XFAD female mice with or without PF068 (n = 10 mice per group). (**J**) LTP, measured as the change in fEPSP, in the CA1 hippocampal region over 140 min in 5XFAD female mice with or without PF068 treatment (15 mg/kg per day for 1 month). Data were analyzed using two-way ANOVA, effects of time, and genotype, $P < 0.0001$; and Sidak's multiple comparisons test with Geisser-Greenhouse correction, $^{***}P < 0.001$ (n = 8 or 9 slices, 4 or 5 mice per group). (**K**) Immunostaining for ThioS, 6E10, and BACE1 in subiculum of 5- to 8-month-old 5XFAD male mice with or without PF068. Scale bars are 50 μm. (**L**) Quantification of area immunostained for ThioS, 6E10, and BACE1 in the subiculum (top row) and cerebral cortex (bottom row); data were analyzed using Student's unpaired t test (n = 6 or 7 per group). (**M**) qRT-PCR of AhR-dependent gene transcripts significantly altered in hippocampus of 5XFAD female mice administered PF068; data were analyzed using two-way ANOVA with Bonferroni post hoc test ($q < 0.05$). (**N**) qRT-PCR of HIF1α-dependent gene transcripts significantly altered in the hippocampus of 5XFAD female mice administered PF068; data were analyzed using two-way ANOVA with Bonferroni post hoc test ($q < 0.05$).

increased multiple HIF1α transcripts involved in glycolytic metabolism (including *Ldha*, *Aldoa*, *Eno1*, *Pdk1*, *Tip1*, *Pkm*, *Pgam1*, and *Pfkfb3*), indicating that IDO1 inhibition transcriptionally regulates glucose metabolism in vivo.

IDO1 inhibition rescues metabolic and hippocampal memory changes in a tau model of AD pathology

Along with brain accumulation of amyloid aggregates, which is considered necessary but not sufficient for AD development (*26*), the second major pathology in AD is accumulation and spread of misfolded tau in several brain areas. Accordingly, we tested the effects of IDO1 inhibition in the PS19 (P301S) tau model of AD pathology, which expresses a mutant form of human microtubule-associated protein tau (MAPT) (*27*). Hippocampal KYN was increased, whereas lactate was decreased, similar to changes observed in the APP models (Fig. 4, A and B, and fig. S6A). Moreover, IDO1 inhibition in PS19 tau mice rescued deficits in spatial memory in the Barnes maze and NOR (Fig. 4, C and D, and fig. S6, B to F) tasks and restored hippocampal LTP in brain slices (Fig. 4E and fig. S6G). Similar to the 5XFAD model, in the PS19 model, IDO1 inhibition normalized increases in hippocampal AhR- and HIF1α-regulated transcripts (Fig. 4F). Although no clear changes in astrocyte activation were noted (fig. S6H), analysis of hippocampal soluble and insoluble tau (total), as well as phosphorylated tau isoforms (Thr^{181} and Thr^{231} phospho-tau), demonstrated that IDO1 inhibition decreased Thr^{231} phospho-tau in both soluble and insoluble tau fractions and Thr^{181} phospho-tau in the insoluble fraction (Fig. 4, G to J). The rescue of hippocampal function and mitigation of pathology across both amyloid and tau models suggests a shared IDO1-driven metabolic defect triggered by both Aβ and tau.

IDO1 disrupts hippocampal glucose metabolism across amyloid and tau pathology models

To better understand the metabolic basis underlying the beneficial effects of IDO1 inhibition, we performed metabolomic analyses of hippocampus from all three preclinical models. We identified 13 metabolites shared across the APP/PS1, 5XFAD, and PS19 models that demonstrated enrichment for glucose metabolism (Fig. 5, A and B). Across both amyloid and tau pathologies, IDO1 inhibition restored multiple glycolytic and TCA cycle intermediates to WT concentrations, consistent with rescue of a central metabolite-deficient state (Fig. 5, C to F and H to J, and figs. S7, A and B, and S8). APP/PS1;$Ido1^{-/-}$ mice also showed a rescue of hippocampal glucose metabolism as compared to APP/PS1 littermates (Fig. 5G). Similar effects were observed in male and female animals (fig. S7, C and D). Taken together, these data indicate that IDO1 inhibition—across both amyloid and tau pathologies—restores hippocampal glucose metabolism, spatial memory, and synaptic plasticity.

To further confirm that IDO1 inhibition could rescue active glucose metabolism in vivo, we carried out an orthogonal approach and infused isotope-labeled ^{13}C-glucose, at a physiologic rate and concentration such that most brain glucose came from the infused glucose, through the carotid artery of APP/PS1 and PS19 mice treated with vehicle or IDO1 inhibitor. The isotopic glucose infusion was sufficiently rapid to render most brain glucose uniformly ^{13}C-labeled (M+6), allowing measurements of incorporation of ^{13}C-labeled glucose into hippocampal glycolytic and TCA metabolites. IDO1 inhibition restored hippocampal intermediate, lactate, and TCA cycle metabolite labeling to control amounts across both amyloid and tau pathologies (Fig. 6, A and B). To visually confirm these changes, we performed matrix-assisted laser desorption ionization (MALDI) imaging (*28*, *29*). Imaging of vehicle and PF068-treated AD mice demonstrated declines in glucose incorporation into glycolytic (fructose 1,6-biphosphate and lactate) and TCA (malate) intermediates in both APP/PS1 amyloid and PS19 tau models. These declines were reversed across both pathologies by IDO1 inhibition with PF068 (Fig. 6, C to F).

IDO1 inhibition rescues lactate-dependent LTP

Based on the in vitro data that demonstrated a role for IDO1 in regulating astrocytic lactate production, we hypothesized that restoration of hippocampal LTP in PF068-treated AD mice might be dependent on lactate produced by astrocytes that is then transferred to neurons. Accordingly, we administered an inhibitor of monocarboxylate transporters MCT1 and MCT2 (AR-C155858) (*30*) to hippocampal slices derived from AD mice treated with vehicle or IDO1 inhibitor. Inhibition of MCT1/2 disrupts lactate transfer from the astrocyte to the neuron (fig. S8D). MCT1/2 inhibition prevented the PF068-mediated rescue of hippocampal LTP in all three AD models (Fig. 7, A to C), suggesting that IDO1 inhibition rescues LTP in a lactate-dependent manner across different pathologies.

In addition, we performed ^{13}C-glucose mass labeling of hippocampal slices from AD model mice treated with PF068 that had undergone electrophysiology testing and examined downstream incorporation of labeled glucose into TCA intermediates in the presence or absence of MCT1/2 inhibitor (Fig. 7, D to F). As shown previously with in vivo mass labeling (Fig. 6), IDO1 inhibition in APP/PS1, 5XFAD, and PS19 hippocampal slices restored concentrations of isotope-labeled citrate and malate, consistent with resumption of glucose flux to the TCA. However, this rescue was completely prevented by MCT1/2 inhibition, suggesting that neurons use lactate in an IDO1-dependent manner across both amyloid and tau pathologies. Thus, inhibition of IDO1 in amyloid and tau models rescued lactate production and uptake into neurons which, in turn, restored synaptic activity.

IDO1 inhibition restores lactate transfer from hAstrocytes to hNeurons derived from individuals with late-onset AD (LOAD)

The APP/PS1, 5XFAD, and PS19 models recapitulate the individual pathologies of rare genetic forms of familial AD and tauopathy. Most AD, however, is late onset (LOAD), with more complex etiologies. To investigate whether KYN concentrations are altered in LOAD, we measured KYN and TRP in well-characterized human postmortem brain tissues that harbored increasing amounts of Braak pathology, the basis for neuropathological diagnosis of AD (*31*). KYN and TRP concentrations were assessed in the middle frontal gyrus, a brain region that demonstrates bilateral gray matter

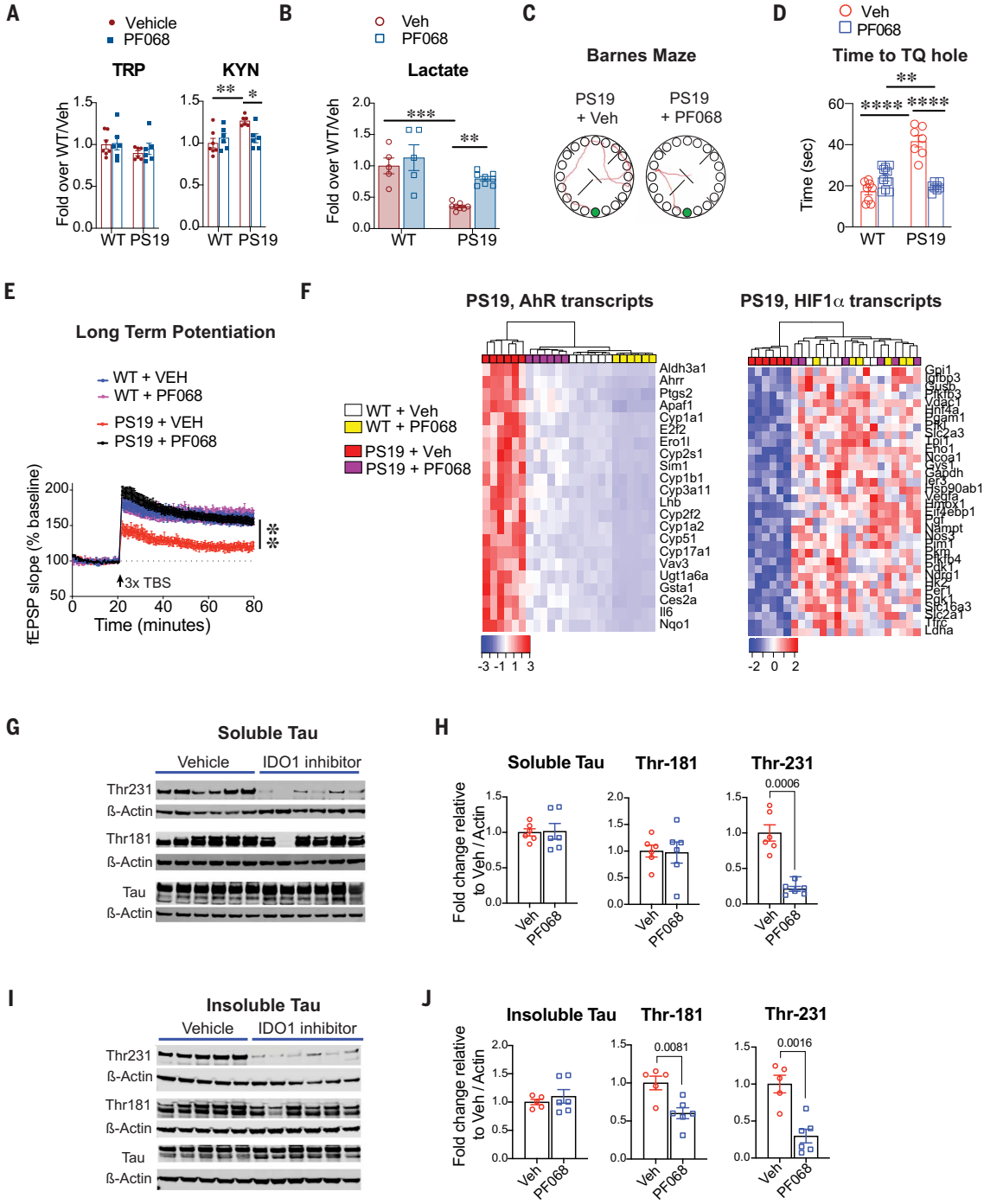

Fig. 4. IDO1 inhibition rescues hippocampal memory and plasticity in mutant Tau PS19 mice. WT and PS19 mice (8 to 9 months old, n = 7 to 10 mice per group, males and females) were treated with vehicle or PF068 (15 mg/kg per day for 1 month). Data are mean ± SEM and were analyzed using two-way ANOVA with Tukey post hoc tests; *P < 0.05, **P < 0.01, ***P < 0.001, and ****P < 0.0001, unless otherwise specified. Hierarchical clustering is represented in terms of distance from the mean, or z-score. (**A**) LC-MS quantification of TRP and KYN in hippocampus of WT and PS19 mice (n = 6 per group). (**B**) Fold change of lactate in the hippocampus of WT and PS19 mice relative to WT with vehicle (n = 5 per group). (**C**) Representative tracings of path to escape hole (green) in PS19 mice with or without PF068 on the day of testing in the Barnes maze. (**D**) Time to the escape hole in the TQ in WT and PS19 mice. (**E**) LTP, measured as the change in fEPSP in the CA1 hippocampal region over 80 min in PS19 mice with or without PF068 treatment (15 mg/kg per day for 1 month). Data were analyzed using two-way ANOVA, effects of time, and genotype, P < 0.0001; and Sidak's multiple comparisons test with Geisser-Greenhouse correction, **P < 0.01 (n = 8 or 9 slices, 4 or 5 mice per group). (**F**) qRT-PCR of AhR-dependent gene transcripts (left heat map) and HIF1α-dependent gene transcripts (right heat map) significantly altered in hippocampus of PS19 mice administered PF068 (q < 0.05). (**G**) Representative immunoblot of hippocampal soluble total tau, Thr^{181} phospho-tau, and Thr^{231} phospho-tau in PS19 mice administered PF068. (**H**) Quantification of soluble total tau, Thr^{181} phospho-tau, and Thr^{231} phospho-tau; data were analyzed using unpaired t test with Welch's correction (n = 5 or 6 mice per group). (**I**) Representative immunoblot of hippocampal sarkosyl-insoluble total tau, Thr^{181} phospho-tau, and Thr^{231} phospho-tau in PS19 mice administered PF068. (**J**) Quantification of sarkosyl-insoluble total tau, Thr^{181} phospho-tau, and Thr^{231} phospho-tau; data were analyzed using unpaired t test with Welch's correction (n = 5 or 6 mice per group).

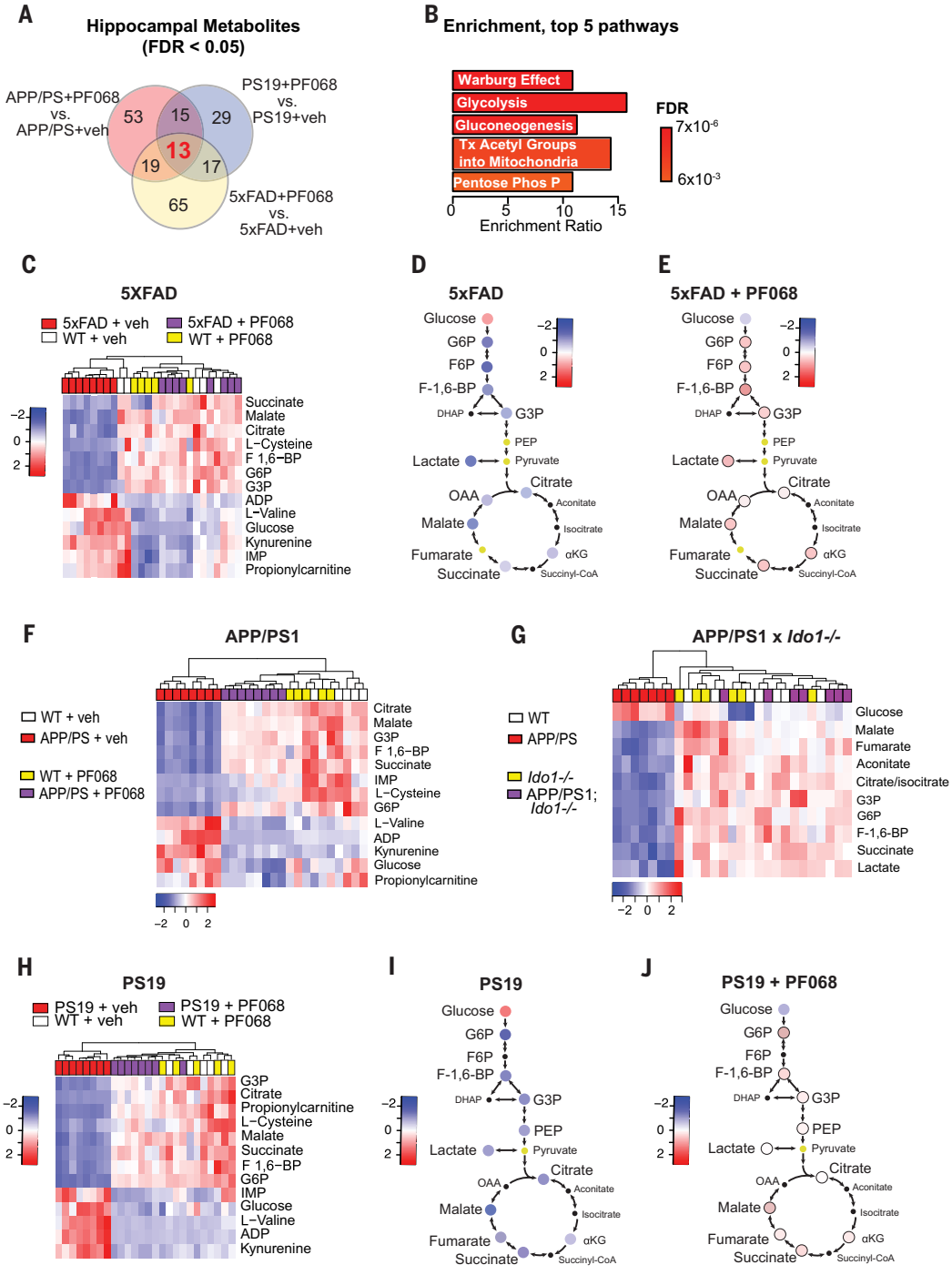

Fig. 5. IDO1 inhibition restores hippocampal glucose metabolism across amyloid and tau pathologies. 5XFAD and WT littermates (5 to 6 months old, female), APP/PS1 and WT littermates (10 to 12 months old, male), PS19 and WT littermates (8 to 9 months old, n = 7 to 10 mice per group, males and females) were treated with vehicle or PF068 (15 mg/kg per day for 1 month). Hierarchical clustering of significantly regulated metabolites [one-way ANOVA, false discovery rate (FDR) < 0.05] is represented in terms of distance from the mean, or z-score. Metabolic maps are represented by the average z-score. (**A**) Venn diagram depicting number of significantly altered metabolites (q < 0.05) detected by untargeted metabolomics from hippocampi in PF068-treated versus vehicle-treated APP/PS1, 5XFAD, and PS19 mice. Thirteen metabolites are shared across the three comparisons of amyloid and tau pathologies. (**B**) Enrichment pathway analysis of 13 shared metabolites from (A) using MetaboAnalyst. (**C**) Hierarchical clustering of the 13 shared hippocampal metabolites in 5XFAD and WT littermates with or without PF068. (**D** and **E**) Schematic depicting amounts of glycolytic and TCA metabolites and their average z-score value from (C). Note the rescue of glycolysis and TCA with IDO1 inhibition in 5XFAD mice. (**F**) Hierarchical clustering of the 13 shared hippocampal metabolites in WT and APP/PS1 littermates with or without PF068. (**G**) Glycolytic and TCA cycle metabolomic profiling of hippocampi isolated from WT (n = 7), *Ido1*$^{-/-}$ (n = 6), APP/PS1 (n = 7), APP/PS1;*Ido1*$^{-/-}$ (n = 7) male littermates at 10 to 12 months of age. (**H**) Hierarchical clustering of the 13 shared hippocampal metabolites in PS19 and WT littermates with or without PF068. (**I** and **J**) Schematic depicting amounts of glycolytic and TCA metabolites and their average z-score value from (H). Note the rescue of glycolysis and TCA with IDO1 inhibition in PS19 mice.

loss (*32*), synaptic loss, and high Aβ burden (*33*). The tissue was obtained from subjects classified as nondemented (Braak I-II, n = 12), demented Braak I-II (non-AD, n = 12), AD Braak III-IV (AD-mid, n = 12), and AD Braak V-VI (AD-high, n = 12). Diagnostic groups were balanced for age, gender, and postmortem interval. Demographic information of the cohort is shown in table S1. Liquid chromatography–mass spectrometry (LC-MS) revealed an increase in KYN, but not TRP, with increasing Braak stage (Fig. 8A).

Next, we asked if the effect of IDO1 on the regulation of glucose metabolism could be modeled in LOAD human astrocytes and neurons in vitro. Patient-specific human iPSC lines were differentiated into pairs of genetically matched neurons (hNeurons) and astrocytes

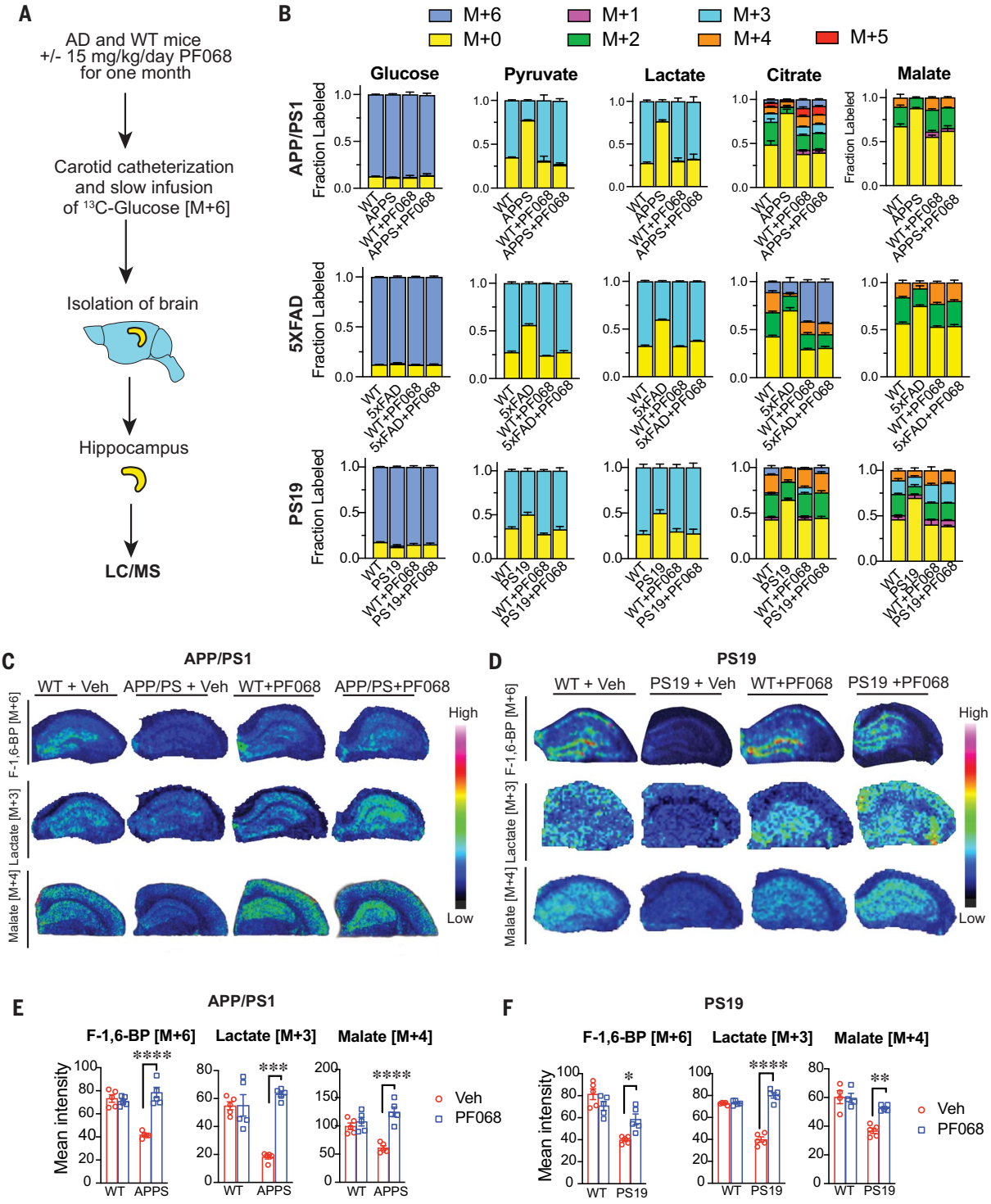

Fig. 6. In vivo mass labeling reveals that IDO1 inhibition rescues glucose incorporation into the TCA cycle in hippocampi of AD model mice. APP/PS1 mice (10 to 12 months old, male, n = 5 mice per group), 5XFAD mice (5 to 6 months old, female, n = 5 mice per group), PS19 mice (8 to 9 months old, male and female, n = 5 mice per group), and age-matched WT littermates were treated with or without PF068 for 1 month. Mice subsequently underwent heavy isotope–labeling experiments and MALDI imaging. Data are mean ± SEM and were analyzed using two-way ANOVA with Tukey post hoc tests; *P < 0.05, **P < 0.01, ***P < 0.001, and ****P < 0.0001. (**A**) Schematic depicting carotid catheterization and infusion of ^{13}C-glucose to achieve steady-state isotope labeling of glucose in vivo in AD model mice. [Figure created with BioRender.com] (**B**) Isotope tracing of ^{13}C-glucose metabolism in hippocampi of APP/PS1 (top row), 5XFAD (middle row), and PS19 (bottom row) mice treated with vehicle or PF068. IDO1 inhibition with PF068 restores glucose incorporation into glycolytic and TCA metabolites across both amyloid and tau pathologies. (**C** and **D**) Representative MALDI images of coronal hippocampal sections from APP/PS1 mice with or without PF068 and PS19 mice with or without PF068 showing rescue in ^{13}C-labeled glycolytic intermediate fructose-1,6-bisphosphate (F-1,6-BP) [M+6], lactate [M+3], and TCA intermediate malate [M+4]. (**E** and **F**) Mean fluorescent intensity (MFI) quantification of (C) and (D).

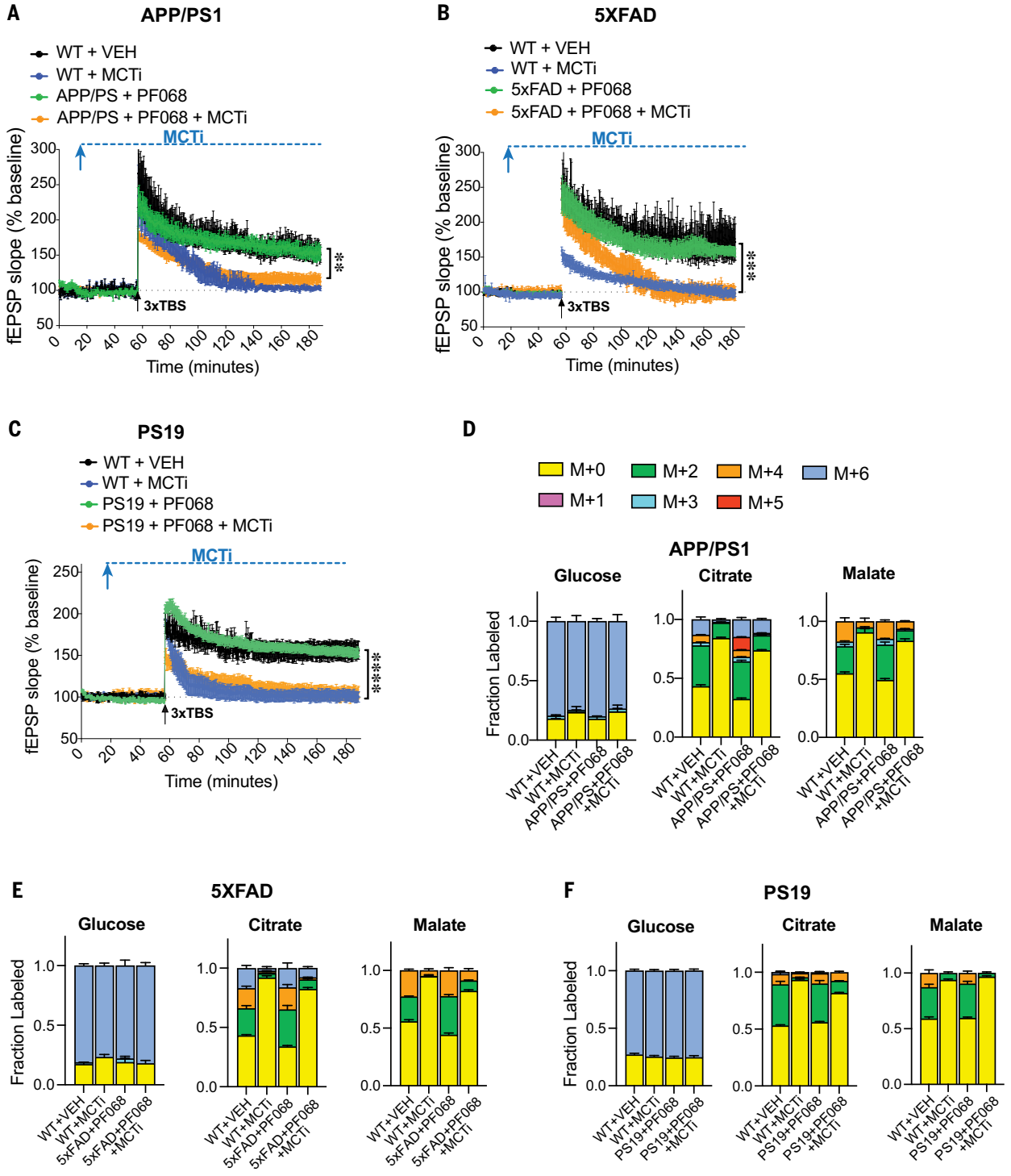

Fig. 7. IDO1 inhibition rescues lactate-dependent LTP in hippocampi of AD model mice. APP/PS1 mice (10 to 12 months old, male), 5XFAD mice (5 to 6 months old, female), PS19 mice (8 to 9 months old, male and female), and WT littermates were treated with or without PF068 (15 mg/kg per day for 1 month), and hippocampal slices were assessed by electrophysiology and mass labeling. Data are mean ± SEM. (**A** to **C**) LTP, measured as the change in fEPSP in the CA1 hippocampal region over 180 min. Hippocampal slices from PF068-treated AD and WT mice were stimulated with monocarboxylate transporter-1/2 inhibitor (MCTi; 50μM) beginning 15 min after the start of the recording (blue arrow) and 45 min before theta-burst stimulation (3×TBS; black arrows) and continuing for the whole recording interval. Data were analyzed using two-way ANOVA, effects of time, and genotype, $P < 0.0001$; and Sidak's multiple comparisons test with Geisser-Greenhouse correction, $^{**}P < 0.01$, $^{***}P < 0.001$, and $^{****}P < 0.0001$ ($n = 8$ or 9 slices per hippocampus). (A) Comparison between APP/PS1 mice with PF068 and APP/PS1 mice with PF068 and MCTi; $^{**}P < 0.01$ ($n = 5$ mice per group). (B) Comparison between 5XFAD mice with PF068 and 5XFAD mice with PF068 and MCTi; $^{***}P < 0.001$ ($n = 6$ mice per group). (C) Comparison between PS19 mice with PF068 and PS19 mice with PF068 and MCTi; $^{****}P < 0.0001$ ($n = 6$ to 8 mice per group). (**D** to **F**) Isotope tracing of ^{13}C-glucose in hippocampal slices that had undergone LTP derived from APP/PS1 (D), 5XFAD (E), and PS19 (F) mice. A rescue in glucose incorporation into the TCA cycle occurs in hippocampi from AD model mice treated with IDO1 inhibitor. This rescue is blocked with administration of MCT1/2 inhibitor ($n = 5$ mice per group, 50 μM MCTi).

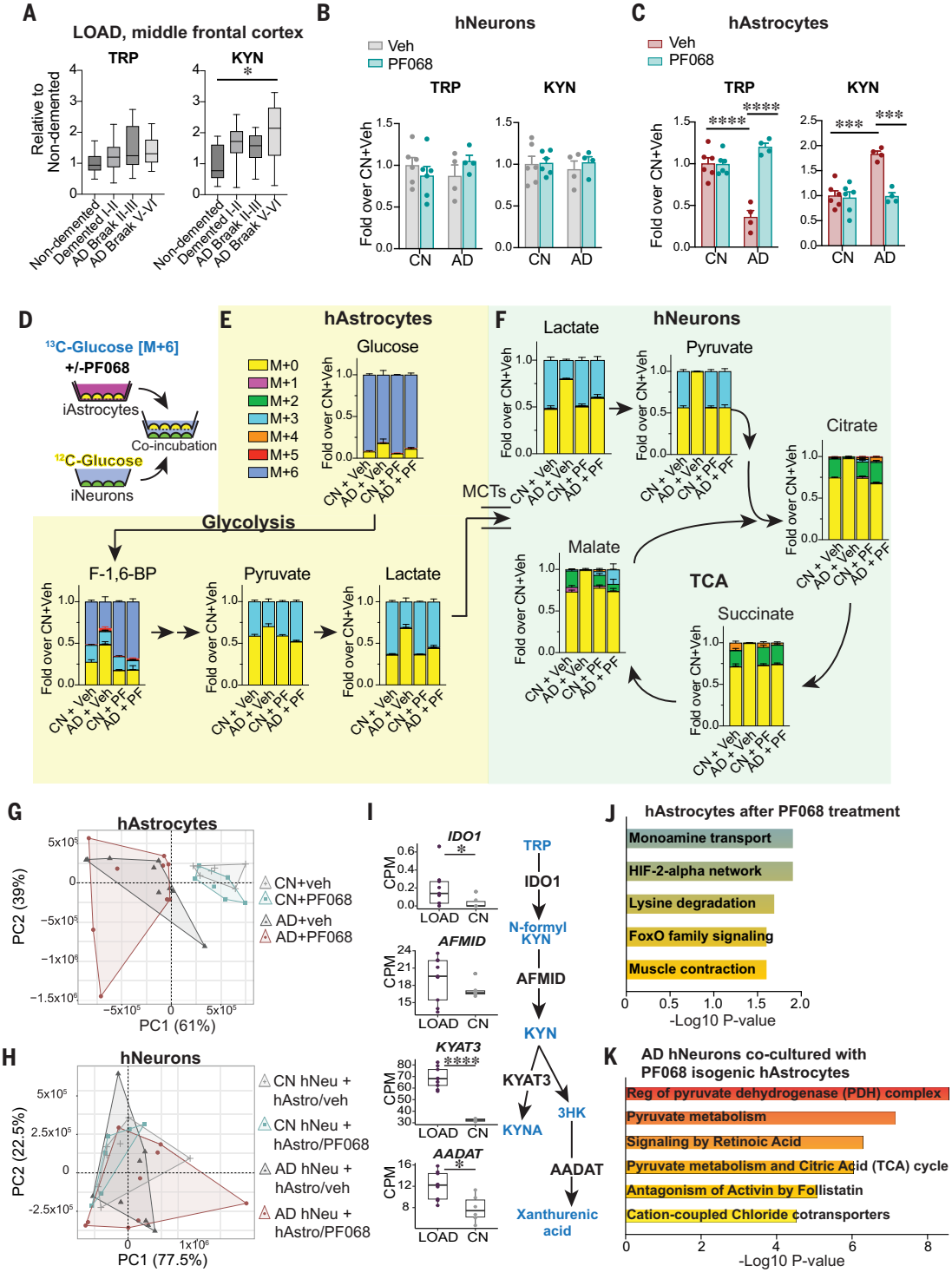

Fig. 8. IDO1 inhibition restores lactate transfer from hAstrocytes to hNeurons in LOAD. (**A**) LC-MS quantification of TRP and KYN in the middle frontal gyrus from nondemented Braak I-II, demented non-AD Braak I-II, AD Braak III-IV, and AD Braak V-VI brain (n = 12 donors per group). Data were analyzed using one-way ANOVA; *P < 0.05. (**B**) LC-MS quantification of TRP and KYN in CN and AD hNeurons (n = 6 CN, n = 4 AD). (**C**) LC-MS quantification of TRP and KYN in CN and AD hAstrocytes (n = 6 CN, n = 4 AD). Data were analyzed using two-way ANOVA with Tukey's post hoc test; ***P < 0.001 and ****P < 0.0001. (**D**) Schematic depicting experimental design for mass labeling of hAstrocytes and subsequent coculture with hNeurons. hAstrocytes were paired with isogenic hNeurons derived from n = 4 AD and n = 6 CN subjects. hAstrocytes from CN and AD patients were labeled with ^{13}C-glucose and stimulated with vehicle or PF068 (100 nM, 20 hours). hAstrocytes on well-inlets were then washed, transferred, and co-incubated with neurons for 4 hours. LC-MS was then performed on cell lysates of hAstrocytes and hNeurons. (**E**) Isotope tracing of ^{13}C-glucose in hAstrocytes with or without PF068 (100 nM, 20 hours) shows rescue of glucose incorporation into glycolytic intermediates and [M+3] lactate (n = 6 CN, n = 4 AD). (**F**) ^{13}C-labeled hAstrocytes from (E) were washed, transferred, and co-incubated with hNeurons for 4 hours. Isotope-labeled astrocytic [M+3] lactate is taken up by hNeurons via the MCT1/2 transporter, and [M+3] lactate metabolism and incorporation into hNeuron pyruvate and TCA intermediates was measured. Glucose flux is restored to that of CN hNeurons in AD hNeurons cocultured with hAstrocytes that had been treated with PF068 (n = 6 CN, n = 4 AD). (**G**) Principal components analysis of RNA-seq DEGs from hAstrocytes derived from CN and AD subjects with or without PF068 (100 nM, 20 hours; n = 2 CN subjects and n = 3 AD subjects, with technical triplicates). (**H**) Principal components analysis of DEGs from CN and AD hNeurons that were cocultured with congenic hAstrocytes stimulated with or without PF068 (100 nM, 20 hours; n = 2 CN and n = 3 AD, with technical triplicates). (**I**) Shown on the left are box plots of kynurenine pathway transcripts from hAstrocytes derived from CN or LOAD subjects. Data were analyzed using Wald test; * P < 0.05 and ****P < 0.001 (n = 2 CN and n = 3 AD, with technical triplicates). Shown on the right is a diagram of the kynurenine pathway highlighting enzymatic steps corresponding to transcripts increased in LOAD hAstrocytes. (**J**) Top significantly enriched gene ontology terms in LOAD hAstrocytes of transcripts significantly regulated by PF068 versus vehicle. CPM, counts per million. (**K**) Top significantly enriched gene ontology terms from differentially regulated transcripts in LOAD hNeurons cocultured with isogenic hAstrocytes that had been treated with PF068 versus vehicle. Note enrichment of pyruvate and TCA metabolic pathways.

(hAstrocytes) (fig. S9, A and B). We performed LC-MS quantification of TRP and KYN from hNeurons and hAstrocytes derived from cognitively normal (CN) individuals and individuals with LOAD. We observed no changes in hNeuron TRP, KYN, or downstream kynurenine pathway metabolites between CN and LOAD individuals. However, hAstrocytes showed reduced TRP and increased KYN in LOAD individuals compared with those in CN individuals (Fig. 8, B and C, and fig. S9, C and D). Incubating LOAD astrocytes with the IDO1 inhibitor PF068 normalized concentrations of TRP and KYN, suggesting increased IDO1 activity in LOAD astrocytes compared with CN astrocytes.

We then tested the effect of IDO1 inhibition on the regulation of glucose metabolism and lactate transfer in hAstrocytes co-incubated with hNeurons from CN individuals and those with LOAD. We labeled hAstrocytes with ^{13}C-glucose and treated with either vehicle or PF068 for 20 hours. The hAstrocytes were washed completely and then transferred into a coculture with their respective isogenic hNeurons for 4 hours to allow hAstrocyte-generated [M+3] lactate to be taken up by hNeurons (Fig. 8D). Glucose metabolism was reduced in LOAD hAstrocytes compared with CN hAstrocytes; however, this deficit was normalized after IDO1 inhibition (Fig. 8E and fig. S9E). In particular, [M+3] lactate in AD hAstrocytes, which was reduced compared with CN hAstrocytes, was restored to CN concentrations with PF068. Upon co-incubation of PF068-treated hAstrocytes with hNeurons, [M+3] lactate uptake in hNeurons was also normalized (Fig. 8F and fig. S9F). Co-incubation of LOAD hNeurons with PF068-treated hAstrocytes restored glucose incorporation into pyruvate and downstream TCA metabolites. Application of exogenous lactate to CN and LOAD neurons in the presence of an MCT1 inhibitor confirmed that lactate is a substrate for downstream generation of TCA metabolites in human iPSC-derived neurons (iNeurons) (fig. S9G). Taken together, these findings suggest that IDO1 generation of KYN suppresses lactate production in LOAD hAstrocytes and subsequent uptake by hNeurons. IDO1 inhibition restored glucose flux in hAstrocytes, which enabled lactate uptake in LOAD hNeurons, replenishing the TCA that fuels mitochondrial respiration and synaptic activity.

The metabolic rescue induced by IDO1 inhibition in LOAD astrocytes and neurons resembled that observed in the hippocampus of our preclinical mutant APP and Tau models. To identify potential mechanisms underlying this in vitro effect, we performed RNA sequencing (RNA-seq) on a subset of our LOAD and CN human iPSC cohort. Principle components analysis indicated a robust disease status signature and mild drug effect in LOAD hAstrocytes, but no significant differences in hNeurons, regardless of disease status or drug treatment (Fig. 8, G and H). Gene expression was evaluated for every condition and revealed differentially expressed genes (DEGs) in vehicle-treated LOAD versus CN hAstrocytes that included genes encoding kynurenine pathway enzymes (Fig. 8I). Although the transcriptional effect of PF068 was relatively modest, gene ontology analysis of LOAD neurons cocultured with genetically matched, PF068-treated hAstrocytes demonstrated changes in pathways associated with increased pyruvate utilization and TCA function, similar to what we observed in preclinical models of AD (Fig. 8, J and K, and fig. S10, A and B). Motif analysis on DEGs from comparisons between LOAD and CN hAstrocytes revealed a specific enrichment of the AhR-ARNT motif (fig. S10C). Unbiased hierarchical clustering of AhR-ARNT–associated transcripts identified by motif analysis demonstrated separation of AhR target genes between LOAD and CN hAstrocytes (fig. S10D), suggesting a role for the IDO1 pathway and KYN generation in regulating astrocytic responses in LOAD.

Discussion

In this study, we combined in vitro and in vivo preclinical models to explore the role of astrocytes in AD pathogenesis. We identified the kynurenine pathway, and specifically IDO1-generated KYN, as a suppressor of astrocytic glucose metabolism and metabolic support of neurons. In vitro, activation of IDO1 in astrocytes by Aβ and tau oligomers, two major pathologic effectors in AD, increased KYN and suppressed glycolysis and lactate production, an effect that was blocked with a pharmacological IDO1 inhibitor. In vivo, IDO1 blockade reversed amyloid- and tau-mediated disruption of hippocampal glycolysis, spatial memory, and LTP. IDO1-dependent suppression of astrocyte lactate production was also observed in human astrocytes derived from AD but not CN subjects. Isotope labeling demonstrated that IDO1 inhibition of hAstrocytes restored the uptake and metabolism of astrocytic [M+3] lactate in cocultured hNeurons. In human postmortem frontal cortex, cerebral KYN rose with increasing Braak AD stages, in line with the observation of increased IDO1-derived hippocampal KYN in APP/PS1, 5XFAD, and PS19 preclinical models. Taken together, our data suggest that increased IDO1 activity and KYN generation across amyloid and tau pathologies suppress hippocampal glucose metabolism, spatial memory, and synaptic plasticity. Restoring astrocytic glucose metabolism with IDO1 inhibition may represent an alternative therapeutic modality for neurodegenerative diseases such as AD that is distinct from present amyloid-lowering strategies.

In vitro, $A\beta_{42}$ and tau oligomers disrupted astrocytic bioenergetics in an IDO1-dependent manner, where induction of KYN led to nuclear translocation of AhR and activation of AhR:ARNT gene transcription. Blockade of KYN production with an IDO1 inhibitor conversely activated HIF1α:ARNT transcription of glycolytic genes and restored astrocyte glucose metabolism and production of lactate. In vivo, mutant APP and tau transgenic mouse models that were administered an IDO1 brain-penetrant inhibitor or APP/PS1 mice that had a genetic deletion of *Ido1* showed reduced hippocampal KYN and reciprocally increased lactate. As in primary astrocytes, hippocampal AhR and HIF1α gene expression was regulated similarly by IDO1 across both amyloid and tau pathologies. Confirmatory in vivo mass labeling of the hippocampus with ^{13}C-glucose demonstrated that IDO1 inhibition and reduction of KYN restored glucose incorporation into lactate and TCA metabolites. Indeed, slice electrophysiology combined with mass labeling indicated that the rescue of LTP by IDO1 inhibition in APP/PS1, 5XFAD, and PS19 hippocampal slices was dependent on functional MCT1/2 transporters that carry lactate from astrocytes to neurons.

The characteristic spatial distribution of glucose hypometabolism in parietal and temporal cortex by fluorodeoxyglucose–positron emission tomography (FDG-PET) has enabled clinical differentiation of AD from other dementias. At a molecular level, recent proteomic studies provide some insight into this clinical observation by identifying disruptions in glucose metabolism, notably in microglia and astrocytes (*4*). One limitation of our study is that we did not investigate the effects of IDO1 in brain microglia, which have been previously shown to have increased expression in AD (*34*). KYN produced by microglia could potentially be taken up by astrocytes, where it would suppress astrocyte glucose metabolism. Alternatively, elevated KYN production in microglia could lead to increased generation of the downstream metabolite quinolinic acid (QA), an agonist of the *N*-methyl-D-aspartate (NMDA) receptor and a potential neurotoxin. Although one outcome of inhibiting IDO1 activity could be decreased generation of downstream neuroactive kynurenine pathway metabolites kynurenic acid (KYNA) and QA (*35*), we did not observe PF068-dependent changes in these metabolites in vitro in astrocytes or neurons or in hippocampi from mutant APP and tau models. The beneficial effect of IDO1 inhibition in vivo on astrocytic glucose metabolism was also associated with a reduction in dense core and diffuse amyloid plaque in 5XFAD mice and a reduction of phosphorylated tau isoforms in the PS19 model. A change in distribution of amyloid suggests an effect on microglia, which play an important role in amyloid plaque formation. Phosphorylated tau reduction suggests that the overall metabolic health of the neuron may influence the activity of kinases and phosphatases that modify the tau phosphorylation state.

Astrocytes perform essential functions, including facilitating synapse formation and plasticity, transporting glucose and other molecules from blood via the endothelium, immune surveillance, and maintenance of neurotransmitter pools. Although neurons can use glucose, astrocytes also provide fuel for neuronal activity in the form of lactate derived from glucose or glycogen (*19*, *21*, *36*). IDO1 blockade rescued synaptic potentiation across amyloid and tau pathologies in an MCT1/2-dependent fashion, indicating that astrocytic lactate transfer to neurons is regulated by astrocytic IDO1. We explored whether this relationship also occurred in congenic human astrocyte-neuron pairs derived from control and AD subjects. Here, astrocytes from individuals with AD diverged from controls in their production of KYN and in regulation of induction of the kynurenine pathway and AhR-regulated transcripts. Although we cannot explain why the AD signature was only observed in hAstrocytes and not hNeurons, we have controlled for purity of glial progenitor cells and hAstrocytes, and the yield and time to generate colonies were similar across CN and LOAD iPSC lines. Because these experiments did not involve $A\beta_{42}$ or tau oligomers, the difference between LOAD and CN hAstrocytes may be cell intrinsic, potentially reflecting genetic or epigenetic differences between CN and AD disease states. Labeling with ^{13}C-glucose confirmed that IDO1 inhibition rescued AD hAstrocyte glycolysis and lactate generation. In cocultures of human astrocytes and neurons derived from AD subjects, deficient astrocyte lactate transfer to neurons was corrected by IDO1 inhibition, resulting in improved neuronal metabolism.

In addition to uncovering a critical role of IDO1 in brain glucose metabolism, our study highlights the potential of IDO1 inhibitors, developed as an adjunctive therapy for cancer, to be repurposed for neurodegenerative diseases such as AD. This study also reveals a more general mechanism contributing to neuronal dysfunction that cuts across distinct pathologies. In addition to AD, manipulation of IDO1 may be relevant to Parkinson's disease dementia (*37*), which is characterized by amyloid accumulation in addition to α-synuclein, as well as the broad spectrum of tauopathies. There is the possibility that deficient astrocytic glucose metabolism could also underlie other neurodegenerative diseases that are characterized by the accumulation of other misfolded proteins where increases in kynurenine pathway metabolites have been observed (*38*).

Methods summary

A full description of the methods can be found in the supplementary materials. The supplementary materials and methods section includes descriptions of primary cell cultures; compounds and proteins; mouse models and behavioral assessments; immunocytochemistry; amyloid and tau quantification; quantitative polymerase chain reaction (PCR); bioenergetic measurements; electrophysiology; transcriptomics metabolic experiments, including mass labeling and MALDI; and statistical analyses.

REFERENCES AND NOTES

1. D. S. Knopman *et al*., Alzheimer disease. *Nat. Rev. Dis. Primers* **7**, 33 (2021). doi: 10.1038/s41572-021-00269-y; pmid: 33986301
2. S. Dewanjee *et al*., Altered glucose metabolism in Alzheimer's disease: Role of mitochondrial dysfunction and oxidative stress. *Free Radic. Biol. Med.* **193**, 134–157 (2022). doi: 10.1016/j.freeradbiomed.2022.09.032; pmid: 36206930
3. D. A. Butterfield, B. Halliwell, Oxidative stress, dysfunctional glucose metabolism and Alzheimer disease. *Nat. Rev. Neurosci.* **20**, 148–160 (2019). doi: 10.1038/s41583-019-0132-6; pmid: 30737462
4. E. C. B. Johnson *et al*., Large-scale proteomic analysis of Alzheimer's disease brain and cerebrospinal fluid reveals early changes in energy metabolism associated with microglia and astrocyte activation. *Nat. Med.* **26**, 769–780 (2020). doi: 10.1038/s41591-020-0815-6; pmid: 32284590
5. C. S. von Bartheld, J. Bahney, S. Herculano-Houzel, The search for true numbers of neurons and glial cells in the human brain: A review of 150 years of cell counting. *J. Comp. Neurol.* **524**, 3865–3895 (2016). doi: 10.1002/cne.24040; pmid: 27187682
6. G. A. Dienel, Brain glucose metabolism: Integration of energetics with function. *Physiol. Rev.* **99**, 949–1045 (2019). doi: 10.1152/physrev.00062.2017; pmid: 30565508
7. A. E. Waitt, L. Reed, B. R. Ransom, A. M. Brown, Emerging roles for glycogen in the CNS. *Front. Mol. Neurosci.* **10**, 73 (2017). doi: 10.3389/fnmol.2017.00073; pmid: 28360839
8. P. Mächler *et al*., In vivo evidence for a lactate gradient from astrocytes to neurons. *Cell Metab.* **23**, 94–102 (2016). doi: 10.1016/j.cmet.2015.10.010; pmid: 26698914
9. M. Platten, E. A. A. Nollen, U. F. Röhrig, F. Fallarino, C. A. Opitz, Tryptophan metabolism as a common therapeutic target in cancer, neurodegeneration and beyond. *Nat. Rev. Drug Discov.* **18**, 379–401 (2019). doi: 10.1038/s41573-019-0016-5; pmid: 30760888
10. C. A. Opitz *et al*., An endogenous tumour-promoting ligand of the human aryl hydrocarbon receptor. *Nature* **478**, 197–203 (2011). doi: 10.1038/nature10491; pmid: 21976023
11. C. R. Dostal, N. S. Gamsby, M. A. Lawson, R. H. McCusker, Glia- and tissue-specific changes in the Kynurenine Pathway after treatment of mice with lipopolysaccharide and dexamethasone. *Brain Behav. Immun.* **69**, 321–335 (2018). doi: 10.1016/j.bbi.2017.12.006; pmid: 29241670
12. H. S. Suh *et al*., Astrocyte indoleamine 2,3-dioxygenase is induced by the TLR3 ligand poly(I:C): mechanism of induction and role in antiviral response. *J. Virol.* **81**, 9838–9850 (2007). doi: 10.1128/JVI.00792-07; pmid: 17626075
13. M. de Majo *et al*., Granulin loss of function in human mature brain organoids implicates astrocytes in TDP-43 pathology. *Stem Cell Reports* **18**, 706–719 (2023). doi: 10.1016/j.stemcr.2023.01.012; pmid: 36827976
14. B. Gomes *et al*., Characterization of the selective indoleamine 2,3-dioxygenase-1 (IDO1) catalytic inhibitor EOS200271/PF-06840003 supports IDO1 as a critical resistance mechanism to PD-(L)1 blockade therapy. *Mol. Cancer Ther.* **17**, 2530–2542 (2018). doi: 10.1158/1535-7163.MCT-17-1104; pmid: 30232146
15. A. Bessede *et al*., Aryl hydrocarbon receptor control of a disease tolerance defence pathway. *Nature* **511**, 184–190 (2014). doi: 10.1038/nature13323; pmid: 24930766
16. M. Mandl, R. Depping, Hypoxia-inducible aryl hydrocarbon receptor nuclear translocator (ARNT) (HIF-1β): Is it a rare exception? *Mol. Med.* **20**, 215–220 (2014). doi: 10.2119/molmed.2014.00032; pmid: 24849811
17. S. J. Kierans, C. T. Taylor, Regulation of glycolysis by the hypoxia-inducible factor (HIF): Implications for cellular physiology. *J. Physiol.* **599**, 23–37 (2021). doi: 10.1113/JP280572; pmid: 33006160
18. C. M. Alberini, E. Cruz, G. Descalzi, B. Bessières, V. Gao, Astrocyte glycogen and lactate: New insights into learning and memory mechanisms. *Glia* **66**, 1244–1262 (2018). doi: 10.1002/glia.23250; pmid: 29076603
19. A. Suzuki *et al*., Astrocyte-neuron lactate transport is required for long-term memory formation. *Cell* **144**, 810–823 (2011). doi: 10.1016/j.cell.2011.02.018; pmid: 21376239
20. J. Duran *et al*., Lack of astrocytic glycogen alters synaptic plasticity but not seizure susceptibility. *Mol. Neurobiol.* **57**, 4657–4666 (2020). doi: 10.1007/s12035-020-02055-5; pmid: 32770452
21. P. J. Magistretti, I. Allaman, Lactate in the brain: From metabolic end-product to signalling molecule. *Nat. Rev. Neurosci.* **19**, 235–249 (2018). doi: 10.1038/nrn.2018.19; pmid: 29515192
22. D. R. Borchelt *et al*., Accelerated amyloid deposition in the brains of transgenic mice coexpressing mutant presenilin 1 and amyloid precursor proteins. *Neuron* **19**, 939–945 (1997). doi: 10.1016/S0896-6273(00)80974-5; pmid: 9354339
23. A. L. Oblak *et al*., Comprehensive evaluation of the 5XFAD mouse model for preclinical testing applications: A MODEL-AD study. *Front. Aging Neurosci.* **13**, 713726 (2021). doi: 10.3389/fnagi.2021.713726; pmid: 34366832
24. S. Viana da Silva *et al*., Early synaptic deficits in the APP/PS1 mouse model of Alzheimer's disease involve neuronal adenosine A_{2A} receptors. *Nat. Commun.* **7**, 11915 (2016). doi: 10.1038/ncomms11915; pmid: 27312972
25. N. Jain, C. A. Lewis, J. D. Ulrich, D. M. Holtzman, Chronic TREM2 activation exacerbates Aβ-associated tau seeding and spreading. *J. Exp. Med.* **220**, e20220654 (2023). doi: 10.1084/jem.20220654; pmid: 36219197
26. E. S. Musiek, D. M. Holtzman, Three dimensions of the amyloid hypothesis: Time, space and 'wingmen'. *Nat. Neurosci.* **18**, 800–806 (2015). doi: 10.1038/nn.4018; pmid: 26007213
27. Y. Yoshiyama *et al*., Synapse loss and microglial activation precede tangles in a P301S tauopathy mouse model. *Neuron* **53**, 337–351 (2007). doi: 10.1016/j.neuron.2007.01.010; pmid: 17270732
28. M. Nakamura *et al*., Quantitative MALDI-MS/MS assay for serum cortisol through charged derivatization. *J. Pharm. Biomed. Anal.* **178**, 112912 (2020). doi: 10.1016/j.jpba.2019.112912; pmid: 31610394
29. Y. Sugiura *et al*., Visualization of in vivo metabolic flows reveals accelerated utilization of glucose and lactate in penumbra of ischemic heart. *Sci. Rep.* **6**, 32361 (2016). doi: 10.1038/srep32361; pmid: 27581923
30. M. J. Ovens, A. J. Davies, M. C. Wilson, C. M. Murray, A. P. Halestrap, AR-C155858 is a potent inhibitor of monocarboxylate transporters MCT1 and MCT2 that binds to an intracellular site involving transmembrane helices 7-10. *Biochem. J.* **425**, 523–530 (2010). doi: 10.1042/BJ20091515; pmid: 19929853
31. H. Braak, E. Braak, Neuropathological stageing of Alzheimer-related changes. *Acta Neuropathol.* **82**, 239–259 (1991). doi: 10.1007/BF00308809; pmid: 1759558
32. P. M. Thompson *et al*., Cortical change in Alzheimer's disease detected with a disease-specific population-based brain atlas. *Cereb. Cortex* **11**, 1–16 (2001). doi: 10.1093/cercor/11.1.1; pmid: 11113031
33. J. Clinton, S. E. Blackman, M. C. Royston, G. W. Roberts, Differential synaptic loss in the cortex in Alzheimer's disease: A study using archival material. *Neuroreport* **5**, 497–500 (1994). doi: 10.1097/00001756-199401120-00032; pmid: 8003683
34. G. J. Guillemin, B. J. Brew, C. E. Noonan, O. Takikawa, K. M. Cullen, Indoleamine 2,3 dioxygenase and quinolinic acid immunoreactivity in Alzheimer's disease hippocampus. *Neuropathol. Appl. Neurobiol.* **31**, 395–404 (2005). doi: 10.1111/j.1365-2990.2005.00655.x; pmid: 16008823
35. Y. S. Huang, J. Ogbechi, F. I. Clanchy, R. O. Williams, T. W. Stone, IDO and kynurenine metabolites in peripheral and CNS disorders. *Front. Immunol.* **11**, 388 (2020). doi: 10.3389/fimmu.2020.00388; pmid: 32194572
36. R. A. Swanson, M. M. Morton, S. M. Sagar, F. R. Sharp, Sensory stimulation induces local cerebral glycogenolysis: Demonstration by autoradiography. *Neuroscience* **51**, 451–461 (1992). doi: 10.1016/0306-4522(92)90329-Z; pmid: 1465204
37. D. J. Irwin, V. M. Lee, J. Q. Trojanowski, Parkinson's disease dementia: Convergence of α-synuclein, tau and amyloid-β pathologies. *Nat. Rev. Neurosci.* **14**, 626–636 (2013). doi: 10.1038/nrn3549; pmid: 23900411
38. D. C. Maddison, F. Giorgini, The kynurenine pathway and neurodegenerative disease. *Semin. Cell Dev. Biol.* **40**, 134–141 (2015). doi: 10.1016/j.semcdb.2015.03.002; pmid: 25773161
39. P. S. Minhas, K. I. Andreasson, Restoring hippocampal glucose metabolism rescues cognition across Alzheimer's disease pathologies. Dryad (2024); https://doi.org/10.5061/dryad.dbrv15f9j.

ACKNOWLEDGMENTS

We thank the Stanford Behavioral and Functional Laboratory, the Stanford Mass Spectroscopy Core, and the Stanford Neuroscience Microscopy Service. We thank the study participants and staff of

the Shiley-Marcos University of California, San Diego (UCSD) Alzheimer's Disease Center. Fig. S8D was created with Biorender.com. **Funding:** This work was supported by National Institutes of Health (NIH) grants RO1AG048232 (K.I.A.), RF1AG058047 (K.I.A.), and P30 AG0066515 (K.I.A.); the Princeton Catalysis Initiative and NIH grant 1DP1DK113643; American Heart Foundation grants 19PABH1345800 (K.I.A.) and 19PABHI34610000 (F.H.G.); the Phil and Penny Knight Initiative for Brain Resilience at the Wu Tsai Neurosciences Institute, Stanford University (K.I.A.); NIH grant 5T32GM007365-45 (P.S.M.); the French-American Foundation for Medical Research and Education (P.S.M.); the Paul and Daisy Soros Fellowship for New Americans (P.S.M.); the Gerald J. Lieberman Fellowship (P.S.M.); NIH grants RF1 AG056306 (F.H.G.) and R37 AG072502-03 (F.H.G.); the JPB Foundation (F.H.G.); the Milky Way Research Foundation (F.H.G.); Howard Hughes Medical Institute (HHMI) Hanna H. Gray Fellows Program GT15655 (M.R.M.); the Burroughs Wellcome Fund PDEP 1022694 (M.R.M.); the Scully Initiative (A.L.-H., F.M.L.); the Jean Perkins Foundation (F.M.L.); the Taube Family Foundation (F.M.L.); the AMED-Moonshot Program (Y.S. and M.S.); and the Wu Tsai Neurosciences Knight Initiative for Brain Resilience Scholar Award (T.U. and H.E.). Data and tissue were obtained from the Arizona Study of Aging and Neurodegenerative Disorders (AZSAND), which is supported by National Institute of Neurological Disorders and Stroke (NINDS) grant U24 NS072026, National Institute on Aging (NIA) grant P30 AG19610, the Arizona Department of Health Services, the Arizona Biomedical Research Commission, and the Michael J. Fox Foundation for Parkinson's Research. Human iPSCs were derived by the Salk Stem Core Facility, which is supported by NIA grant P30 AG062429. K.I.A. is a Chan Zuckerberg–San Francisco Biohub Investigator. **Author contributions:** P.S.M., A.S.D., Q.W., J.C., T.C., H.E., Y.J.J., Y.A.A., and M.M. designed and performed experiments and analyzed the data. S.D.M. characterized the APP-PS1; *Ido1*$^{-/-}$ mice. R.G., T.N., K.H., A.K., and J.R.J. performed, analyzed, and interpreted data from hNeurons and hAstrocyte experiments, and F.H.G. supervised human iPSC experiments. J.R.J. performed and analyzed RNA sequencing. T.U. and M.W. generated iAstrocytes. A.L.-H. and F.M.L. performed and analyzed electrophysiology experiments. T.Y. advised on tau isolation and aided with preparation. E.N.W., E.M.U., G.E.S., and T.G.B. advised and provided postmortem brain tissue. Y.S. and M.S. carried out MALDI analyses. P.P., B.C.J., L.L., and M.R.M. performed metabolomics and isotope tracing. J.D.R. advised on metabolomic methods. M.R.M. supervised metabolomics experiments. P.S.M. and K.I.A. conceived and supervised the project, designed the experiments, interpreted the data, and wrote the manuscript. **Competing interests:** K.I.A. is a co-founder, board member, and consultant for Willow Neuroscience, Inc. F.M.L. is a founder of, board member of, and consultant for and has financial interest in PharmatrophiX, a company focused on small-molecule development for treatment of neurodegenerative disorders. **Data and materials availability:** The data that support the findings of this study are available on Dryad (*39*). The Gene Expression Omnibus (GEO) accession number for the RNA-seq data is GSE245823.

SUPPLEMENTARY MATERIALS

science.org/doi/10.1126/science.abm6131
Materials and Methods
Figs. S1 to S10
Table S1
References (*40*–*73*)
MDAR Reproducibility Checklist

Submitted 9 October 2023; accepted 25 June 2024
10.1126/science.abm6131